




## RESEARCH ARTICLE

# Chemo-small extracellular vesicles released in cisplatin-resistance ovarian cancer cells are regulated by the lysosomal function

Cristóbal Cerda-Troncoso<sup>1,2,3</sup>  | Felipe Grünenwald<sup>2</sup> | Eloísa Arias-Muñoz<sup>1</sup> |  
 Viviana A. Cavieres<sup>1,4</sup> | Albano Caceres-Verschae<sup>2</sup> | Sergio Hernández<sup>1</sup> |  
 Belén Gaete-Ramírez<sup>2</sup> | Francisca Álvarez-Astudillo<sup>2</sup> | Rodrigo A. Acuña<sup>5</sup> |  
 Matias Ostrowski<sup>6</sup> | Patricia V. Burgos<sup>1,3</sup>  | Manuel Varas-Godoy<sup>2,3,7</sup> 

<sup>1</sup>Organelle Phagy Lab, CEBICEM, Facultad de Medicina y Ciencia, Universidad San Sebastián, Santiago, Chile

<sup>2</sup>Cancer Cell Biology Lab, CEBICEM, Facultad de Medicina y Ciencia, Universidad San Sebastián, Santiago, Chile

<sup>3</sup>Centro Ciencia & Vida, Fundación Ciencia & Vida, Santiago, Chile

<sup>4</sup>Departamento de Ciencias Biológicas y Químicas, Facultad de Medicina y Ciencia, Universidad San Sebastián, Santiago, Chile

<sup>5</sup>Centro de Medicina Regenerativa, Facultad de Medicina, Clínica Alemana Universidad del Desarrollo, Santiago, Chile

<sup>6</sup>Facultad de Medicina, Instituto de Investigaciones Biomédicas en Retrovirus y Sida (INBIRS), Universidad de Buenos Aires (UBA), Buenos Aires, Argentina

<sup>7</sup>Advanced Center for Chronic Diseases, Santiago, Chile

## Correspondence

Patricia V. Burgos, Organelle Phagy Lab, CEBICEM, Facultad de Medicina y Ciencia, Universidad San Sebastián, Carmen Sylva 2444, Providencia, Chile. Email: [patricia.burgos@uss.cl](mailto:patricia.burgos@uss.cl)

Manuel Varas-Godoy, Cancer Cell Biology Lab, CEBICEM, Facultad de Medicina y Ciencia, Universidad San Sebastián, Carmen Sylva 2444, Providencia, Chile. Email: [manuel.varas@uss.cl](mailto:manuel.varas@uss.cl)

**Current Affiliation:** Cristóbal Cerda-Troncoso, Department of Human Genetics, KU Leuven, Leuven, Belgium.

Albano Caceres-Verschae, Department of Oncology/Pathology, Karolinska Institutet, Stockholm, Sweden.

## Funding information

Fondo de Financiamiento de Centros de Investigación en Áreas Prioritarias, Grant/Award Number: 1513001I; Agencia Nacional de Investigación y Desarrollo, Grant/Award Number: FB210008; Fondo Nacional de Desarrollo Científico y Tecnológico, Grant/Award Numbers: Doctoral fellowship 21230341, Postdoctoral fellowship 3200825, Postdoctoral fellowship 3220485, Regular Grant 1171649, Regular Grant 1190928, Regular Grant 1211261, Regular Grant 1230983

## Abstract

Chemoresistance is a common problem in ovarian cancer (OvCa) treatment, where resistant cells, in response to chemotherapy, secrete small extracellular vesicles (sEVs), known as chemo-sEVs, that transfer resistance to recipient cells. sEVs are formed as intraluminal vesicles (ILVs) within multivesicular endosomes (MVEs), whose trafficking is regulated by Ras-associated binding (RAB) GTPases that mediate sEVs secretion or lysosomal degradation. A decrease in lysosomal function can promote sEVs secretion, but the relationship between MVEs trafficking pathways and sEVs secretion in OvCa chemoresistance is unclear. Here, we show that A2780cis cisplatin (CCDP) resistant OvCa cells had an increased number of MVEs and ILVs structures, higher levels of Endosomal Sorting Complex Required for Transport (ESCRTs) machinery components, and RAB27A compared to A2780 CDDP-sensitive OvCa cells. CDDP promoted the secretion of chemo-sEVs in A2780cis cells, enriched in DNA damage response proteins. A2780cis cells exhibited poor lysosomal function with reduced levels of RAB7, essential in MVEs-Lysosomal trafficking. The silencing of RAB27A in A2780cis cells prevents the Chemo-EVs secretion, reduces its chemoresistance and restores lysosomal function and levels of RAB7, switching them into an A2780-like cellular phenotype. Enhancing lysosomal function with rapamycin reduced chemo-sEVs secretion. Our results suggest that adjusting the balance between secretory MVEs and lysosomal MVEs trafficking could be a promising strategy for overcoming CDDP chemoresistance in OvCa.

## KEYWORDS

chemo-EVs, chemoresistance, lysosomal function, ovarian cancer, RAB27A

This is an open access article under the terms of the [Creative Commons Attribution-NonCommercial-NoDerivs License](https://creativecommons.org/licenses/by-nc-nd/4.0/), which permits use and distribution in any medium, provided the original work is properly cited, the use is non-commercial and no modifications or adaptations are made.

© 2024 The Author(s). *Journal of Extracellular Biology* published by Wiley Periodicals LLC on behalf of International Society for Extracellular Vesicles.

## 1 | INTRODUCTION

The World Health Organization reported that around 18.1 million women worldwide had cancer, and 9.6 million died due to this disease (Bray et al., 2018). Ovarian cancer (OvCa) is one of the most common gynecologic cancers (Sung et al., 2021). The current treatment for OvCa involves primary debulking surgery followed by platinum-based and/or taxane-based combination chemotherapy (Kim et al., 2018; Reid et al., 2017). For platinum-based, cisplatin (CDDP) is the most used chemotherapy (Dasari & Tchounwou, 2014; Helm & States, 2009), however, a significant percentage of sensitive cells develop chemoresistance (Galluzzi et al., 2012; Shen et al., 2012).

The acquisition of chemoresistance depends on the adaptive responses of the tumor cells to evade the effects of chemotherapy (Qin et al., 2020; Tchounwou et al., 2021). In OvCa, CDDP-chemoresistance encompasses a reduction in the entry of CDDP into cells, DNA repair mechanisms, metabolic reprogramming, cell death inhibition and epigenetic changes (Ai et al., 2016; Chan et al., 2021; Norouzi-Barough et al., 2018; Patch et al., 2015; Tchounwou et al., 2021; Tong et al., 2019; Xie et al., 2021). Additionally, small extracellular vesicles (sEVs), which play a crucial role in intercellular communication by the secretion of proteins and genetic material, contribute significantly (Mathieu et al., 2021). Importantly, different models of chemoresistant cells, including those in OvCa, secrete chemo-sEVs in response to chemotherapy (Wang et al., 2023; Wang et al., 2019). These chemo-sEVs possess a specific cargo profile that facilitates the transfer of chemoresistance to sensitive tumoural cells (Bandari et al., 2020; Safaei et al., 2005; Tian et al., 2022; Yáñez-Mó et al., 2015).

sEVs encompass a variety of vesicle types, including exosomes, that are formed intracellularly as intraluminal vesicles (ILVs) by the inward budding of the endosomal limiting membrane during the process of multivesicular endosomes (MVEs) maturation, organelles that fused with the plasma membrane (PM) causing the secretion of sEVs to the extracellular space (Dixon et al., 2023). The biogenesis of ILVs is mediated by endosomal sorting complex required for transport (ESCRT) machinery and mechanisms supported by specific lipids and scaffold proteins (Ceramide-Sphingomyelin, Tetraspanins and Syndecan–Syntenin–ALIX dependent pathways) (Andreu & Yáñez-Mó, 2014; Baietti et al., 2012; Verderio et al., 2018; Wollert & Hurley, 2010). The transport, tethering, and fusion of MVEs with the PM are regulated by the RAB family small GTPases, molecules that cycle between GTP-bound active and GDP-bound inactive states (Cavieres et al., 2020; Kelly et al., 2012). RAB27A is one of the most studied small GTPases in this process and controls the trafficking and fusion of MVEs with the PM and the release of sEVs under basal and inducible conditions (Dorayappan et al., 2018; Ostrowski et al., 2010). Interestingly, RAB27A has been demonstrated to promote chemoresistance in different types of cancer models by a mechanism related to its role in exosomal secretion (Hertzman Johansson et al., 2013; Li, Jin et al., 2017; Li, Wang et al., 2017; Liu et al., 2017). However, whether CDDP-chemoresistance in OvCa depends on RAB27A function, remains unexplored.

MVEs are also key organelles in the endo-lysosomal degradative pathway. Here, MVEs fused with the lysosomes to degrade the cargo that gets incorporated into ILVs (Huotari & Helenius, 2011; Klumperman & Raposo, 2014), a pathway governed by RAB7 (Bucci et al., 2000; Vanlandingham & Ceresa, 2009), a small GTPase that contributes to the maintenance and biogenesis of lysosomes (Bae et al., 2019; Huotari & Helenius, 2011). The mechanisms that control the trafficking of MVEs to either the PM or in route to lysosomes are only partially understood (Eitan et al., 2016). It is well-established that inhibiting the trafficking of MVEs in one direction can stimulate the alternative pathway as a compensatory response (Adams et al., 2021; Eitan et al., 2016; Guix et al., 2021; Huang et al., 2022; Miranda et al., 2018; van de Vlekkert et al., 2019; Villarroya-Beltri et al., 2016; Zhang et al., 2021). In the context of controlling chemo-sEVs secretion in OvCa cells, targeting a specific MVE trafficking pathway (either secretory or lysosomal degradation) can impact the balance between the two, potentially influencing the secretion of chemo-sEVs. It is particularly proposed that this regulation depends on lysosome function (Izco et al., 2022). Thus, the role of lysosomes in sEVs secretion during cisplatin resistance in OvCa cells has been poorly explored.

Here, we studied the role of MVEs, ILVs and sEVs in the chemoresistance of OvCa by characterizing a cellular model sensitive to CDDP (A2780) and one resistant to it (A2780cis). Compared to A2780, A2780cis exhibits an increased number of ILVs and higher levels of RAB27A, correlating with a higher sEVs secretion and transfer of chemoresistance capacity in response to CDDP. Conversely, A2780cis cells show poor lysosomal function and low protein levels of RAB7. Collectively, these findings suggest that the high number of MVEs and ILVs in A2780cis leads to sEVs secretion in a scenario of lysosomal dysfunction. Importantly, silencing of RAB27A converts A2780cis cells to an A2780-like phenotype, promoting lysosomal function and restoring RAB7 levels. To mimic the effects of RAB27A silencing, we treated the cells with rapamycin, which promotes lysosomal biogenesis. The results showed that co-treating with CDDP and rapamycin blocks the secretion of chemo-sEVs. In conclusion, we propose that the function of chemo-sEVs in OvCa is determined by an imbalance between MVE trafficking pathways, where the levels of RAB27A and RAB7, as well as the lysosomal status, controlled by mTORC1, play critical roles.

## 2 | MATERIALS AND METHODS

### 2.1 | Antibodies

The following monoclonal antibodies were used: anti-ALIX (cat# sc-53540), anti-RAB7 (cat# sc-376362), anti-RAB11A (cat# sc-166912) and anti- $\beta$ -actin (cat# sc-47778) from Santa Cruz Biotechnology (Dallas, TX, USA); anti-CD63 (cat# ab8219), anti-GRP94 (cat# ab90458), anti-RAB22A (cat# ab137093), anti-TSG101 (cat# ab83) and anti-ULK1 (cat# ab128859) from Abcam (Cambridge, UK); anti-LAMP1 clone H4A3 (cat# DSHB-H4A3) from Developmental Studies Hybridoma Bank (Iowa City, IA, USA); anti-GM130 (cat# 610823) and anti-TSG101 (cat# 612696) from BD Bioscience (Becton, NJ, USA); anti-Syntenin 1 (cat# NBP2-76873) from Novous Biological (Littleton, Ontario, Canada); anti-ULK1 S317 (cat# 127535) from Cell Signaling Technology (Danvers, MA, USA). The following polyclonal antibodies: anti-Cathepsin D (cat# AF1014) from R&D Systems (Minneapolis, MN, USA); anti-CD63 (cat# AM11837) from Ango (San Ramon, CA, USA); anti-HGS (HRS) (cat# ab15539) from Abcam; anti-LAMP2A clone AMC2 (cat# 51-2200) from Gibco™ ThermoFisher Scientific (Waltham, MA, USA); anti-RAB35 (cat# 9690) from Cell Signaling Technology; anti-RAB27A (cat# 168013) from Synaptic Systems (Göttingen, Germany). Horseradish peroxidase-conjugated secondary antibodies were purchased from Jackson ImmunoResearch Laboratories (West Grove, PA, USA), and Alexa fluorophore-conjugated secondary antibodies were purchased from Invitrogen™ ThermoFisher Scientific (Carlsbad, CA, USA).

### 2.2 | Plasmids and oligos

The shRNA for RAB27A was cloned in pLKO.1 (Sigma-Aldrich, cat# SHC007), and described in our previous report (Gerber et al., 2015). As a control, we used a shRNA against Luciferase (Sigma-Aldrich, Saint Louis, MO, USA; cat# SHC007). The following sequences were used as a shRNA target shRNA-Luciferase: 5'-CGCTGAGTACTTCGAAATGTC-3', and shRNA-RAB27A: 5'-CGGATCAGTTAAGTGAAGAAA-3'. The packaging plasmids pCMV-VSV-g (cat# 8454) and pS-PAX2 (cat# 12260) was obtained from Addgene (Watertown, MA, USA). The following primers for qPCR were ordered from Integrated DNA Technologies IDT (Coralville, IA, USA). *Glyceraldehyde 3-phosphate dehydrogenase (GAPDH)*: 5'-GGAAGATGGTGTGATGGGATTC-3', 3'-GAAGGTGAAGGTCGGAGTCAA-5'; *RAB27A*: 5'-ATGGAACGGTGTGTGGACAA-3', 3'-CCACATGCCCTTTCTCCTT-5'; and *RAB7* 5'-GACAAGTGCCACAAAGCG-3', 3'-GCATTCCGTGCAATCGTCTG-5'.

### 2.3 | Cell culture

We produced lentivirus using HEK 293T cell line Lenti-X™ 293T from Takara Bio (San Jose, CA, USA; cat# 632180) known for its high transfection efficiency and constitutively expression of the simian virus 40 (SV40) large T antigen for greater lentivirus production efficiency (Merten et al., 2016). HEK 293T cells were cultured in DMEM High Glucose (DMEM-HG) from Cytiva (Marlborough, MA, USA; cat# SH30243.02), supplemented with 10% heat-inactivated FBS (Sartorius, Göttingen, Niedersachsen, Germany), penicillin 100 U/mL, and streptomycin 100 mg/mL (Gibco™ ThermoFisher Scientific), according to the supplier's recommendations. The endometroid carcinoma OvCa A2780 CDDP-sensitive (cat# 93112519) and A2780cis CDDP-resistant (cat# 93112517) cell lines, both obtained from the European Collection of Authenticated Cell Cultures, Sigma-Aldrich, commonly used to investigate CDDP resistance in OvCa (Mad-Adam et al., 2022). These cell lines were cultured in RPMI 1640 (cat# SH30255.02, Cytiva, Marlborough, MA, USA), supplemented with 10% heat-inactivated fetal bovine serum (FBS), penicillin 100 U/mL and streptomycin 100 mg/mL according to supplier's recommendations. To maintain the resistance of A2780cis cells to CDDP (Sigma-Aldrich; cat# 479306), cells were treated with 1  $\mu$ M CDDP every two weeks in culture or every three passages (Mad-Adam et al., 2022). The resistance to CDDP of A2780cis cells compared with A2780 cells was tested by sulforhodamine B (SRB) assay.

HEK 293T was seeded at a density of  $2 \times 10^3$  cells/cm<sup>2</sup>, A2780 and A2780cis cells and  $4 \times 10^3$  cells/cm<sup>2</sup>, respectively. The three cell lines were cultured at 37°C, in a humid environment, and 5% CO<sub>2</sub>. For experiments, each 2–3 days cells were plated after trypsinization with 0.05% Trypsin and 1 mM EDTA (Gibco™, ThermoFisher Scientific) at 37°C. Alternatively, cells were frozen in 1.5 mL of freezing medium (10 % v/v DMSO, 90 % v/v FBS) and stored in cryotubes at –80°C/–150°C.

### 2.4 | Bacterial transformation and plasmid DNA isolation

One Shot™ Stbl3™ *E. coli* cells (Invitrogen™, ThermoFisher Scientific; cat# C7373-03) were used to transform the pLKO.1 shRNA-containing vector following the supplier's recommendations. The plasmid was prepared using the NucleoBond Xtra Midi

kit (Machery-Nagel, Allentown, PA, USA) according to the manufacturer's protocol. The plasmid concentration was quantified using the spectrophotometer EPOCH2 microplate reader (BioTek, Winooski, VT, USA).

## 2.5 | Generation of stable knockdown cell lines with shRNA lentiviral particles

The silencing of RAB27A was achieved by transduction with shRNA-containing lentiviral particles. As a control, cells were transduced with a shRNA targeting luciferase. Lentiviral particles were generated by co-transfection of HEK293T cells with pLKO.1-shRNA, pCMV-VSV-g and pS-PAX2 vector harvested and concentrated as previously described (Varas-Godoy et al., 2018). For transduction, A2780 and A2780cis cells were seeded overnight in 24-well tissue culture plates and then infected with 15  $\mu$ L of the respective concentrated lentivirus, using 1X PBS as control. Cells were cultivated until they reached 80% confluency. After 48 h, the medium was replaced with fresh medium supplemented with 6  $\mu$ g/mL puromycin (Sigma-Aldrich cat# P8833) to select for transduced cells. Cells that developed resistance to puromycin were further expanded and maintained, in a medium containing 3  $\mu$ g/mL puromycin. To check the generation of the stable cell line the silencing of RAB27A was evaluated by qPCR and Western blot.

## 2.6 | Western blot analysis

The preparation of cell lysate protein extracts, SDS-PAGE gels, and Western blots was carried out as previously described (Vargas et al., 2022). For treatments, A2780, A2780cis, A2780-shLuc A2780cis-shLuc and A2780cis-shRAB27A cells were treated with 1  $\mu$ M CDDP, 100 nM rapamycin or a combination of 1  $\mu$ M CDDP and 100 nM rapamycin for 72 h. For sEVs protein extract analysis, 10  $\mu$ g of sEVs were separated by SDS-PAGE gels and then transferred to a polyvinylidene difluoride (PVDF) membrane (ThermoFisher Scientific cat# 88518) for 1 h at 100 V. Further, the membrane was analyzed using protocols previously described (Vargas et al., 2022; Vera et al., 2019).

## 2.7 | RNA isolation and relative quantitative real-time polymerase chain reaction

RNA was isolated from cells using TRIzol (Invitrogen™ cat# 15596018), following the manufacturer's recommendations. RNA yield was quantified using the spectrophotometer EPOCH2 microplate reader (BioTek). Reverse transcription was performed on 2  $\mu$ g of RNA in a 25  $\mu$ L reaction using oligo(dT) and the Moloney Murine Leukemia Virus Reverse Transcriptase Kit (M-MLV RT, cat# M0253S, NEB, Ipswich, MA, USA). Relative Quantitative Real-Time PCR was carried out using 5  $\mu$ L of SsoAdvanced Universal SYBR® Green Supermix (cat# 172571, Bio-Rad, Hercules, CA, USA), 1  $\mu$ L cDNA (1:25 dilution) and 0.6  $\mu$ L of 10  $\mu$ M gene-specific primer mix, totaling a reaction volume of 12  $\mu$ L. Gene expression quantification was conducted using the Rotor-Gene (QIAGEN). The thermal profile of the reaction was: 95°C for 1 min, followed by 40 cycles of 95°C for 10 s, 60°C for 15 s, and 72°C for 20 s. All samples were run in triplicate, at least. The amplification of the sequence of interest was normalized to an endogenous reference gene, GAPDH. Values were expressed as levels of RAB27A or RAB7 relative to GAPDH levels.

## 2.8 | Transmission electron microscopy

A2780 and A2780cis cells were grown on 60 mm cell culture plates and processed and analyzed for transmission electron microscopy (TEM) analysis at the Advanced Microscopy Unit of the Pontificia Universidad Católica de Chile as previously described (Vargas et al., 2022). Isolated sEVs were fixed with paraformaldehyde (PFA), deposited in a TEM Formvar carbon grid, contrasted with uranyl acetate, and analyzed using a Philips Tecnai 12 microscope (Eindhoven, The Netherlands) at 80 kV, following previously described methods (Vargas et al., 2022; Vera et al., 2019). The number of MVEs was quantified considering that correspond to spherical organelles, containing multiple small vesicles, enclosed by a single outer limiting membrane (Altick et al., 2009). The number of small vesicles inside of MVBs selected was considered as the number of ILVs. The quantification of the area of MVEs was performed in FIJI software version 2.1.0 (<http://imagej.net/software/fiji/>) (Schindelin et al., 2012). The images obtained from 20,000 $\times$  were calibrated using the bar scale and using the freehand selection tool, the MVEs were selected. Then with the measure tool, the area from selected MVEs was obtained.



## 2.9 | Indirect immunofluorescence and fluorometric lysosomal assays with fluorescent probes

A2780, A2780cis, A2780-shLuc, A2780cis-shLuc and A2780cis-shRAB27A cells were seeded on glass coverslips pre-treated with L-poly-Lysine (Sigma-Aldrich, cat# 4707). For experiments involving CDDP and rapamycin treatment, 24 h after seeding, A2780cis cells were treated with 1  $\mu$ M CDDP, 100 nM rapamycin or a combination of 1  $\mu$ M CDDP and 100 nM rapamycin for 72 h. Afterward, cells were washed with 1X PBS, 0.1  $\mu$ M CaCl<sub>2</sub> and 1  $\mu$ M MgCl<sub>2</sub>, fixed, permeabilized, and stained using our previously published protocols (Bustamante et al., 2020; Cavieres et al., 2020).

The lysosomal pH was measured using the LysoTracker™ Red DND-99 probe (Invitrogen™, cat# L-7528) as we previously reported (Vargas et al., 2022). The Cathepsin B activity was assessed using the Magic Red® kit (cat# 937, Immunochemistry Technologies, Davis, CA, USA), following the methodology reported previously (Vargas et al., 2022).

## 2.10 | Confocal fluorescence microscopy

Fluorescence microscopy images were obtained from samples prepared using the Indirect immunofluorescence technique described previously (Vargas et al., 2022). These images were acquired using a TCS SP8 laser-scanning confocal microscope (Leica Microsystems, Wetzlar, Germany) equipped with a 63 $\times$  oil immersion objective (1.4 NA), photomultipliers (PMT) and hybrid detectors (HyD) system. Excitation was performed using 405, 488, 561 and 643 nm laser lines, with the Leica Application Suite LAS X software. To prevent spectral bleed-through, images were acquired in sequential mode with identical settings for each channel, ensuring that 16-bit images were acquired without signal saturation. The measurements of the images were executed using ICY software (Quantitative Image Analysis Unit, Institut Pasteur, <http://icy.bioimageanalysis.org/>). A pipeline was developed to fully automate image analysis, employing the following sequential plugins: active contours for cell segmentation, hk-means for threshold detection, and Wavelet Spot Detector for spot detection. For the quantification of Manders' coefficient of colocalization, we utilized FIJI software version 2.1.0 (available at <http://imagej.net/software/fiji/>) (Schindelin et al., 2012), supplemented by the Just Another Colocalization Plugin (JACoP, 2.1.1 version) (Bolte & Cordelières, 2006). The threshold for the images was adjusted in comparison to the control.

## 2.11 | Small extracellular vesicles isolation

For sEVs isolation, 5  $\times$  10<sup>6</sup> A2780, A2780cis, A2780cis shLuc, A2780cis shRAB27A cells were seeded on 100 cm<sup>2</sup> plates in RPMI supplemented with 1% pen-strep and 5% exosome-depleted FBS (Gibco™, cat# A27208-01). Exosome-depleted FBS was used to prevent the isolation of sEVs present in the FBS, as suggested (Théry et al., 2018). For experiments including treatments with CDDP or rapamycin, the cells were treated with 1  $\mu$ M CDDP or a combination of 1  $\mu$ M CDDP and 100 nM Rapamycin for 72 h, as indicated. After 72 h of culture or treatment, sEVs enriched fractions were obtained from the supernatant medium (SM) of the cells by differential ultracentrifugation (dUC), as previously described (Vera et al., 2019). The resulting pellet was resuspended in 1X PBS and stored at  $-80^{\circ}\text{C}$  until further analysis.

## 2.12 | Small extracellular vesicles characterization and analysis

sEVs were characterized by Western blot and TEM as described above (*Western blot analysis* and *TEM section*). Nanoparticles tracking analysis (NTA) was performed using NanoSight NS300 system (Malvern Instruments, Malvern, United Kingdom, Universidad de los Andes), in accordance with previously established protocols (Vera et al., 2019). Measurements were conducted using a 532-nm laser and a 565-nm long pass filter, with the camera set to level 9 and the detection threshold at 3. Prior to analysis, sEVs were diluted in 1X PBS.

## 2.13 | Chemoresistance transference and cell viability assays

For these assays we used a ratio of 50,000 sEVs per cell. After 16 h A2780 sensitive cells were treated with 3  $\mu$ M CDDP for 48 h. Cell viability of A2780 cells after CDDP treatment was evaluated by the Live/Dead Cell Stain Kit (Invitrogen™, ThermoFisher Scientific) by flow cytometry (BD FACS CantoII, Becton, NJ, USA) and using 0.4% trypan blue (cat# 15250-061, Gibco™, ThermoFisher Scientific).

## 2.14 | Mass spectrometry analysis of small extracellular vesicles

sEVs samples were analyzed using SWATH mass spectrometry (MS) to identify differentially expressed proteins. Briefly, 50  $\mu\text{g}$  of sEVs proteins were mixed with RadioImmunoprecipitation Assay Buffer (RIPA) buffer (pH 7.4), sonicated for 15 min, and then centrifuged at  $21,000 \times g$  for 2 min at  $4^\circ\text{C}$ . This process was used to obtain both luminal and membrane-associated proteins from the sEVs. The protein fractions extracted from the sEVs were cleaned-up and concentrated using a 10 kDa Omega filtration centrifuge tubes (PALL, Nanosep). They were reduced, alkylated and digested using the filter-aided sample preparation (FASP) method (Wiśniewski et al., 2009). After digestion, 100  $\mu\text{L}$  of 0.1 % formic acid (FA) was added to the digested samples, which were then loaded onto a 10-kDa-size exclusion membrane (PALL, Nanosep), and centrifuged at  $15,000 \times g$  for 5 min to filter out the peptides. The flow-through containing the peptides was reconstituted in an equal volume of 0.1% trifluoroacetic acid (TFA) in preparation for desalting. The samples were desalted using SOLA $\mu$  HRP solid phase extraction (SPE) 96-well plate (Thermo Fisher Scientific), following the manufacturer's instructions. Finally, the desalted peptides were dried and reconstituted with 50  $\mu\text{L}$  of 0.1% FA in water.

Peptides were separated by liquid chromatography in tandem with MS (LC-MS) using an AB SCIEX 5600 Triple TOF spectrometer (ABSCIEX) coupled to a Nano Ultra ID+ HPLC system (Eksigent). Each sample was loaded onto a reversed-phase trap column (CHROMXP C18CL 5  $\mu\text{m}$ ,  $10 \times 0.3$  mm; Eksigent), and the column was washed for 15 min at a flow rate of 3  $\mu\text{L}/\text{min}$ . This was followed by peptide separation on a reversed-phase analytical column (CHROMXP C18CL 3  $\mu\text{m}$ , 120A0,  $150 \times 0.075$  mm, Eksigent). Peptides were eluted using a linear gradient of buffer A ( $\text{H}_2\text{O}/0.1\%$  FA), and buffer B (Acetonitrile (ACN)/0.1% FA) over 75 min from 10% to 95% mobile phase B at 250 nL/min. The peptides were then introduced into the mass spectrometer via a nanospray ion source (Thermo Fisher). The resulting peptides were analyzed in an information-dependent acquisition (IDA) mode on the AB Sciex TripleTOF 5600 System, utilizing an isolation width of 26 Da (comprising 25 Da for optimal ion transmission efficiency plus 1 Da for window overlap). A set of 32 overlapping windows covered the mass range from 100–2000 m/z.

All mass spectra were analyzed using the Paragon algorithm in ProteinPilot™ Software (V4.5 beta, AB Sciex,) against the *Homo sapiens* Uniprot database. The change in relative abundance of proteins in sEVs was determined by comparing the extracted-ion peak intensities of two technical replicates for each sample, utilizing the SWATH Acquisition Microapp (version 2.0) within PeakView (version 2.2) (Alharbi et al., 2021). A false discovery rate (FDR) analysis was applied during the processing method, setting the detected protein threshold to 0.05 (equivalent to a 10% FDR). Venn diagram illustrating the shared proteins identified across different sEVs groups was generated using the BioInfoRX Venn Diagram Plotter (<https://bioinforx.com/apps/venn.php>). Data underwent Gene Set Enrichment Analysis (GSEA) and Gene ontology analysis using the Webgestalt (<http://www.webgestalt.org/>), while Protein-Protein Interaction Networks Functional Enrichment Analysis was conducted using STRING (<https://string-db.org/>). The mass spectrometry work was carried out at the University of Queensland Center for Clinical Research (UQCCR), Brisbane, Australia.

## 2.15 | Sulforhodamine B assay for the determination of the lethal dose 50 (LD<sub>50</sub>)

Cells were cultured in 96 well tissue culture plates. 6 h post-seeding, various doses of CDDP were tested, and cells were incubated at  $37^\circ\text{C}$ , in a humidified atmosphere with 5%  $\text{CO}_2$  for 24 h. Then, cells were fixed with a 20% trichloroacetic acid solution at  $4^\circ\text{C}$  for 1 h. After fixation, the cells were washed four times in distilled water, completely removing the wash volume each time. Cells were then stained with 100  $\mu\text{L}$  of 0.4% SRB (dissolved in 0.1% acetic acid. SRB, Sigma-Aldrich, cat# 230162) at room temperature for 1 h, followed by four washes with 1% acetic acid. After air-drying overnight, 100  $\mu\text{L}$  of 10 mM Tris-base solution was added to each well, and the plates were agitated on an orbital shaking for 30 min. Absorbance at 492 nm was measured using an EPOCH2 microplate reader (BioTek). LD<sub>50</sub> values, reflecting CDDP's cytotoxic effects, were computed using Prism 9.0 (GraphPad Software, San Diego, CA, USA) employing a non-linear regression model with a variable slope (log(agonist) vs. response). Two-way ANOVA was utilized to assess differences between cell viability curves.

## 2.16 | Quantifications and statistical analysis

Densitometric quantification of Western blot images was performed using FIJI software (version 2.1.0 (<http://imagej.net/software/fiji/>)) (Schindelin et al., 2012). Protein bands were quantified from at least three independent experiments for each condition. Data analysis, including densitometric quantifications, real-time qPCR, electron microscopy transmission, fluorescence confocal microscopy and SRB-LD<sub>50</sub> was conducted using Microsoft Excel 2022 (Microsoft Corporation) and Prism 9.0 (GraphPad Software) on macOS Big Sur. This facilitated the generation of charts and the performance of statistical analyses. Results are presented in graphs showing the mean  $\pm$  standard error of the mean (SEM). Statistical significance was assessed

using parametric one-tailed *t*-test and non-parametric one-tailed Mann–Whitney tests, as appropriate for each figure. *p*-values of \**p* < 0.05, \*\**p* < 0.01 and \*\*\**p* < 0.001 were considered statistically significant and are indicated in the figures. For mass spectrometry data, unpaired Student's *t*-tests were applied, with *p* < 0.05 deemed statistically significant.

More details are in the extended methods section.

### 3 | RESULTS

#### 3.1 | A2780cis cells have increased protein machinery for ILVs biogenesis and exosome secretion

To investigate whether the chemoresistance phenotype in A2780cis (CDDP-resistant) cells could be linked to changes in MVEs and ILVs, we analyzed the presence of CD63-positive punctated structures. CD63 was used as a marker of MVEs compartments (Kobayashi et al., 2000; Vanlandingham & Ceresa, 2009; White et al., 2006), in comparison to A2780 CDDP-sensitive (A2780) OvCa cells (Figure 1a). We found by immunofluorescence confocal analysis that A2780cis cells have a higher number of CD63-positive punctated structures per cell than A2780 cells (Figure 1a,b). In addition, CD63-positive punctated structures show an increased area in A2780cis cells compared to A2780 cells (Figure 1a,c). This initial finding prompted us to investigate whether A2780cis could have a higher capacity in MVEs and ILVs biogenesis (Peng et al., 2021). Specifically, we studied MVEs and ILVs structures by transmission electron microscopy (TEM) in both cell lines (Figure 1d). We found in A2780cis cells that MVEs organelles showed an increased area in comparison to A2780 cells (Figure 1e). Moreover, we observed a higher number of ILVs per MVEs in A2780cis compared to A2780 cells (Figure 1f). These results could indicate that A2780cis cells have an increased capacity to form MVEs and ILVs from *novo* synthesis. To evaluate this possibility, we measured the levels of ESCRT family members involved in ILVs biogenesis, including the hepatocyte growth factor-regulated tyrosine kinase substrate (HRS), the tumour susceptibility gene 101 protein (TSG101) and the programmed cell death 6-interacting protein (ALIX) (Falguières et al., 2008; Wollert & Hurley, 2010). Additionally, we assessed levels of LAMP2A, a *es mejor*: a lysosomal transmembrane protein recently linked to the biogenesis of ILVs and secretion of sEVs (Ferreira et al., 2022). Our western blot analysis revealed that all the proteins evaluated had significantly higher levels in A2780cis cells, compared to A2780 cells (Figure 1g,h). This confirms that CDDP-resistant cells have enhanced protein machinery necessary for ILVs biogenesis. Given the increase in the size of the MVEs and the number of ILVs, which may imply an increased capacity for sEVs secretion, we next examined the levels of key Ras-associated binding (RAB) GTPases known to play critical roles in the secretion of sEVs (Jin et al., 2021; Messenger et al., 2018; Ostrowski et al., 2010; Wang et al., 2014; Wei et al., 2021; Xu et al., 2022). Our results showed that among the RABs evaluated (RAB11A, RAB22A, RAB27A, RAB35), only the levels of RAB27A increased significantly in A2780cis compared to A2780 cells (Figure 1i,j). Since RAB27A has been linked to the secretion of sEVs (Ostrowski et al., 2010), these findings suggest that the CDDP-resistant phenotype in OvCa could be associated with an increased ability of these tumoural cells to increase the biogenesis of MVEs and ILVs, leading to a more secretory state and increased secretion of sEVs.

#### 3.2 | sEVs secreted from A2780cis cells in response to CDDP can transfer cisplatin chemoresistance to recipient A2780 cells

Because A2780cis cells showed a higher level of proteins related to MVEs and ILVs biogenesis and exosome secretion, we investigated if this feature could correlate with the secretion of sEVs which include exosomes. For this, we isolated sEVs by differential centrifugation from supernatant media from A2780 and A2780cis and A2780cis cells treated with 1  $\mu$ M CDDP cultured for 72 h. First, we characterized if the isolated sEVs fractions were enriched on selected exosome markers according to current recommendations (Théry et al., 2018). As expected, we found the sEVs fractions isolated from the three different supernatant media were enriched in endosomal proteins CD63, TSG101 and Syntenin, a scaffold PDZ protein involved in Syndecan-Syntenin-ALIX exosomal biogenesis pathway (Baietti et al., 2012), respecting the total cell lysate (Figure 2a). As an internal sEVs purity control, we measured the levels of the cis-Golgi matrix protein GM130 and the endoplasmic reticulum (ER) luminal protein GRP94, abundant proteins known to be absent in sEVs (Dozio & Sanchez, 2017; Moon et al., 2019). Our analysis showed GM130 and GRP94 were detected only in the total cell lysate (Figure 2a, cell markers). To characterize the isolated sEVs, we analyzed the distribution size of the isolated sEVs fractions in each condition, we performed Nanoparticle Tracking Analysis (NTA). We found all isolated sEVs were enriched in particles between 120 and 200 nm in diameter (Figure 2b). Moreover, the microphotographs show that all sEVs fractions have the typical cup shape morphology (Figure 2c). Collectively, the protocol selected allows the isolation of a mixture of extracellular vesicles enriched in sEVs that present exosome markers (Théry et al., 2018), hereafter indicated for simplicity sEVs. Next, we measured the number of sEVs in each condition by NTA analysis. Unexpectedly, we found that A2780 and A2780cis secreted a similar number of sEVs per cell (Figure 2d). However, treatment of A2780cis with CDDP caused a significant increase in the number of secreted sEVs per cell, compared with untreated cells (Figure 2d). In this regard, it is known that cancer cells secrete sEVs in response to chemotherapeutic agents such as CDDP named chemo-sEVs (Ab Razak

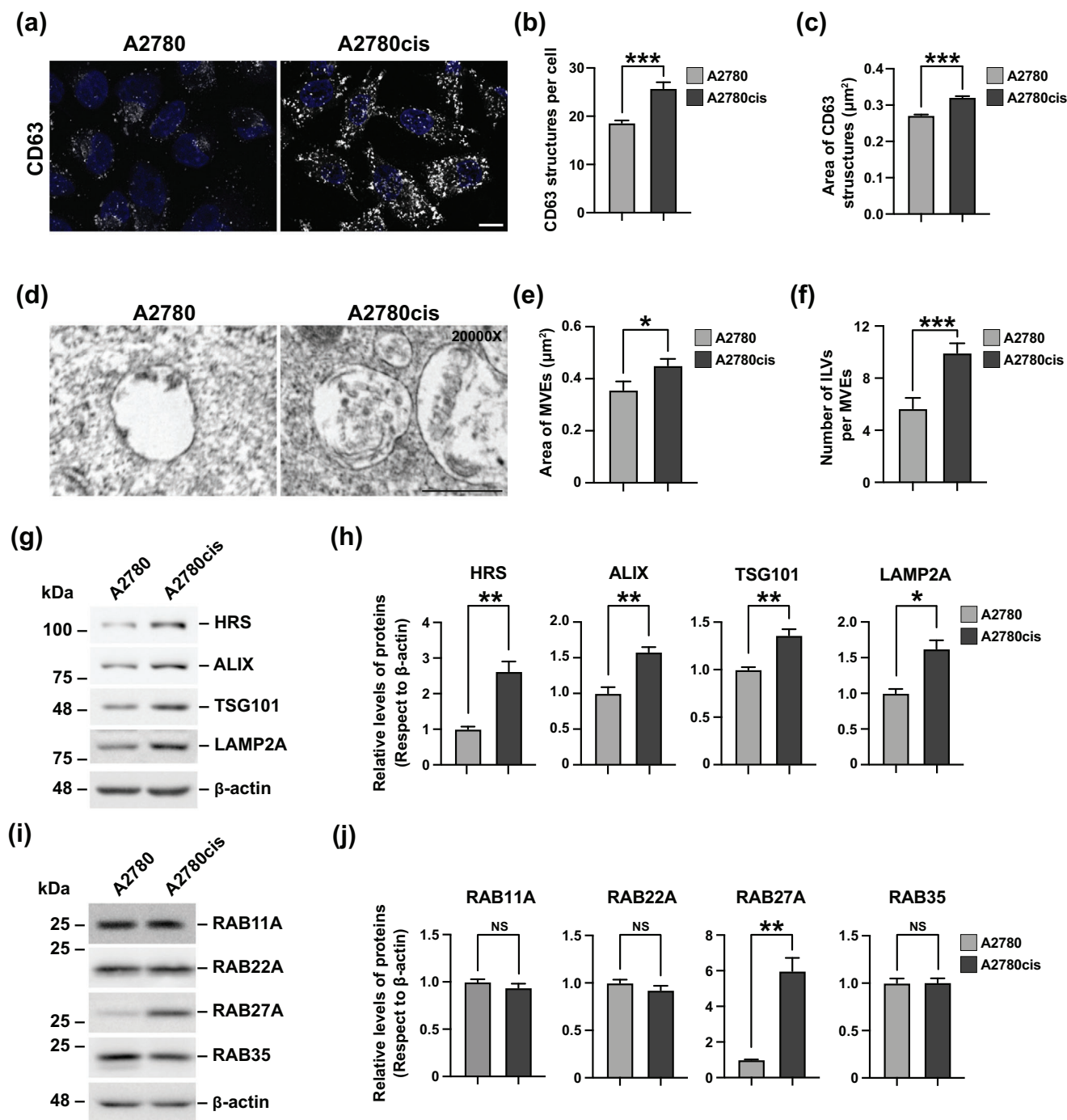


**FIGURE 1** A2780cis CDDP-resistant cells have more capacity to produce and secrete exosomes. (a) Representative confocal microscopy images of A2780 and A2780cis PFA-fixed cells immunofluorescently stained with anti-CD63. Scale Bar 10  $\mu\text{m}$ . (b) Analysis of the number of structures and (c) area of structures of CD63 per cell from images as those shown in (a). Bars indicated the mean with SEM;  $***p < 0.001$ ; one-tailed unpaired parametric *t*-test ( $n > 50$  cells from three independent experiments). (d) Representative TEM micrograph shows MVEs of A2780 and A2780cis cells. Scale Bar 0.5  $\mu\text{m}$ . (e) Semiquantitative analysis of the area of MVEs and (f) ILVs per MVEs of A2780 and A2780cis cells, from images as those shown in (d). Bars indicated the mean with SEM;  $*p < 0.05$ ,  $***p < 0.001$ ; one-tailed, unpaired, parametric *t*-test ( $n > 50$  cells from three independent experiments). (g) Analysis of detergent-soluble protein extracts obtained from A2780 and A2780cis cells by Western blot with anti-HRS, anti-ALIX, anti-TSG101, anti-LAMP2A and anti- $\beta$ -actin. The image is representative of three independent experiments. (h) Densitometric quantification of the signal of HRS, ALIX, TSG101 and LAMP2A from images as those shown in (g). The signal was normalized with  $\beta$ -actin signal. Bars indicated the mean with SEM;  $*p < 0.05$ ,  $**p < 0.01$ , one-tailed, paired, non-parametric Mann-Whitney test ( $n = 3$ ). (i) Analysis of detergent-soluble protein extracts obtained from A2780 and A2780cis cells by Western blot with anti-RAB11A, anti-RAB22A, anti-RAB27A, anti-RAB35 and anti- $\beta$ -actin. The image is representative of three independent experiments. (j) Densitometric quantification of the signal of RAB11A, RAB22A, RAB27A and RAB35 from images as those shown in (i). The signal was normalized with  $\beta$ -actin signal. Bars indicated the mean with SEM;  $**p < 0.01$ , NS: not significant; one-tailed, paired non-parametric Mann-Whitney test ( $n = 3$ ).



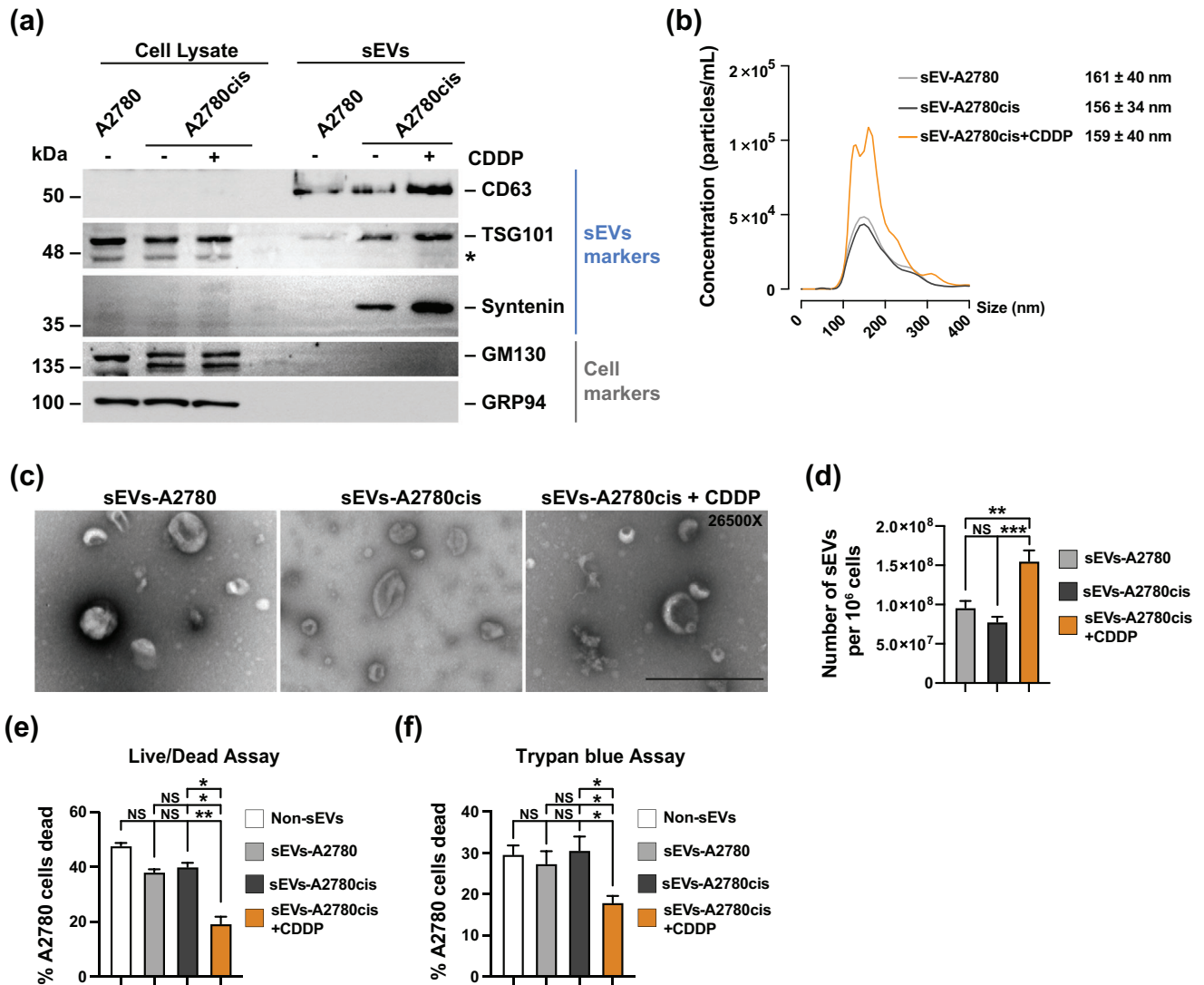


**FIGURE 2** CDDP promotes the secretion of small EVs in A2780cis CDDP-resistant OvCa cells, with chemoresistance transference capacity. (a) Analysis of detergent-soluble protein extracts by Western blot from cell lysates and small EVs (sEVs) obtained by differential ultracentrifugation (dUC) from 72 h supernatant medium (SM) of A2780 (sEVs-A2780), A2780cis (sEVs-A2780cis) and A2780cis cells treated with 1 μM CDDP during 72 h (sEVs-A2780cis+CDDP). To Western blot, we used anti-CD63, anti-TSG101, anti-Syntenin, anti-GM130 and anti-GRP94. \* Indicate unspecified band. (b) Nano-tracking analysis (NTA) of sEVs-A2780, sEVs-A2780cis and sEVs-A2780cis+CDDP obtained by dUC. The quantifications represent the distribution size of the sEVs calculated by the mean concentration of the sEVs of each size ( $n = 5$ . Five independent experiments). (c) Representative images of TEM micrograph of sEVs-A2780, sEVs-A2780cis and sEVs-A2780cis+CDDP, obtained by dUC. ScaleBar 0.5 μm. (d) Analysis of the number of sEVs-A2780, sEVs-A2780cis and sEVs-A2780cis+CDDP per 10<sup>6</sup> cells obtained by dUC. Bars indicated the mean with SEM; \*\* $p < 0.01$ , \*\*\* $p < 0.001$ , NS: not significant; one-tiled, unpaired, non-parametric Man-Whitney test ( $n = 5$ . Five independent experiments). (e,f) Live/Dead cell stain analysis by (e) flow cytometry and (f) trypan blue analysis of A2780 cells treated with 3 μM CDDP for 48 h after 16 h stimulation with PBS (Non-sEVs) or with sEVs-A2780, sEVs-A2780cis and sEVs-A2780cis+CDDP obtained by dUC. The analysis represents the percentage of A2780 cells dead for each condition. Bars indicated the mean with SEM; \* $p < 0.05$ , \*\* $p < 0.01$ , NS: not significant; one-tiled, paired, non-parametric Mann-Whitney test ( $n = 3$ ).

et al., 2019; Bandari et al., 2018), through specific cargos can mediate horizontal transference of drug resistance to drug-sensitive cells (Xavier et al., 2022; Yáñez-Mó et al., 2015).

This feature prompted us to evaluate the potential of these sEVs secreted in response to CDDP, in their capacity to transfer CDDP resistance to chemo-sensitive cells. To do this, we treated A2780cis cells with 1 μM CDDP for 72 h to generate chemo-sEVs and then tested their ability to confer chemo-resistance when incubated with A2780 cells at a ratio of 50,000 chemo-sEVs per cell for 16 h. After, A2780 cells were treated with 3 μM CDDP for 48 h, a concentration that caused approximately 50% mortality after the treatment. Subsequently, the viability of the cells was assessed using both live/dead cell staining analysis by flow cytometry and trypan blue analysis. As controls, A2780 cells were incubated with 50,000 sEVs per cell, which were isolated from either A2780 cells or A2780cis, but without the addition of CDDP. Our results reveal that the chemo-sEVs fraction was effective in significantly reducing CDDP-induced death in A2780 cells compared to the other sEVs fractions, as shown by live/dead staining analysis

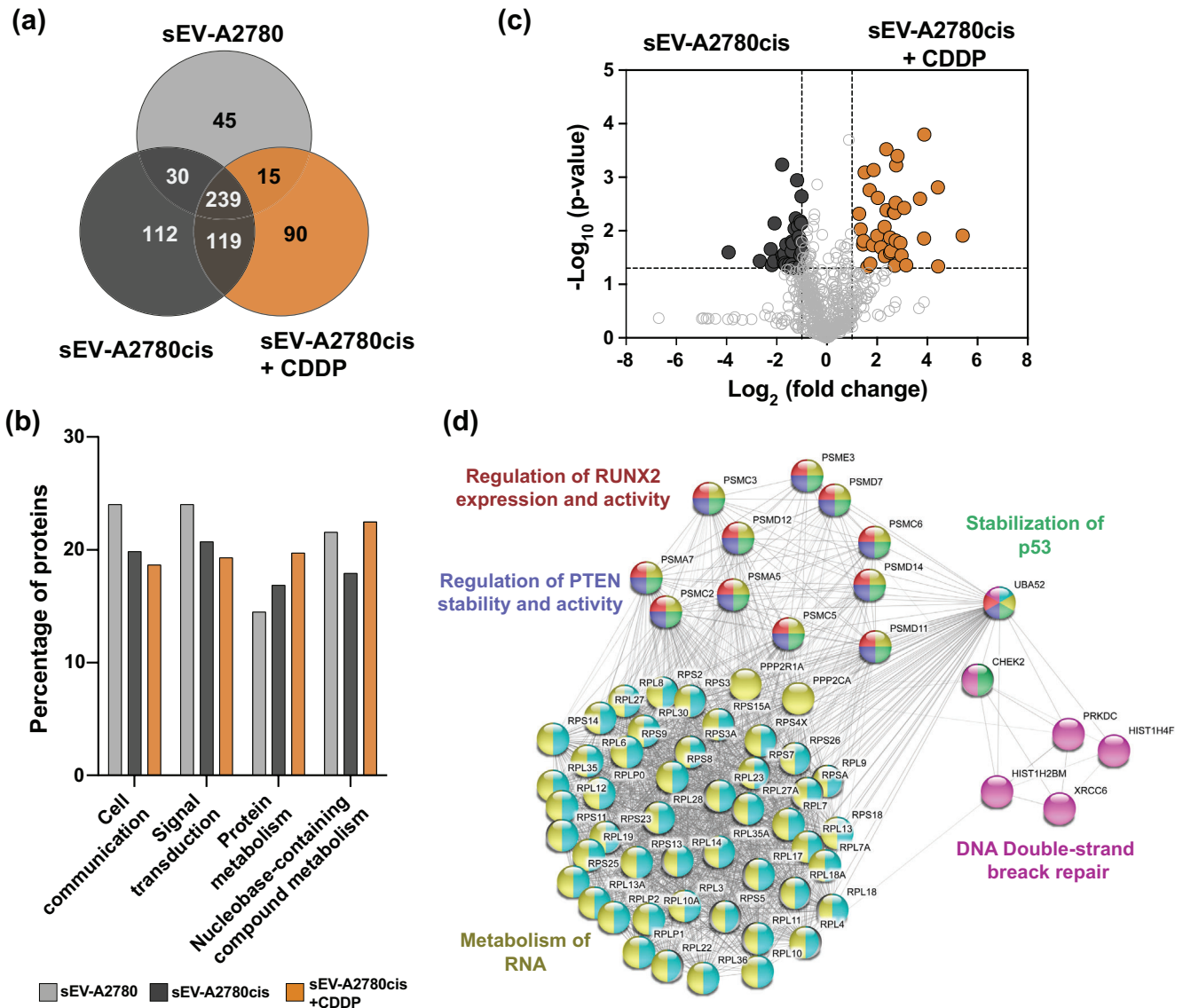


**FIGURE 3** Small EVs protein cargo of A2780cis cells is altered after treatment with CDDP and is enriched with proteins associated with chemoresistance. (a) Venn diagram of proteins from Table S1 identified in sEVs obtained by dUC from 72 h CM of A2780 (sEVs-A2780), A2780cis (sEVs-A2780cis) and A2780cis cells treated with 1  $\mu$ M CDDP during 72 h (sEVs-A2780cis+CDDP). (b) Gene ontology (GO) enrichment analysis of proteins found in sEVs-A2780, sEVs-A2780cis and sEVs-A2780cis+CDDP obtained by dUC. (c) Volcano plot of proteins from Table S2 differentially expressed between sEVs-A2780cis and sEVs-A2780cis+CDDP. (d) Protein-Protein Interaction Networks Functional Enrichment Analysis of total proteins differentially expressed in sEVs-A2780cis+CDDP.

(Figure 2e) and trypan blue analysis (Figure 2f). Therefore, our findings demonstrated the transfer of chemo-sEVs resistance from A2780cis cells by the sEVs to A2780 chemo-sensitive cells, as indicated by the reduction of CDDP-induced cell death.

### 3.3 | sEVs secreted from A2780cis cells in response to CDDP are enriched in proteins involved in chemoresistance

To get insights about which key components of chemo-sEVs could be implicated in the transfer of CDDP chemo-resistance in A2780 chemo-sensitive cells, we performed SWATH mass spectrometry (MS) to identify specific proteins present in those sEVs isolated from A2780cis in response to CDDP (Figure 3). A total of 329, 500, and 463 proteins were identified in the sEVs fractions isolated from A2780, A2780cis and A2780cis+CDDP, containing 45, 112 and 90 proteins exclusive in each group, respectively (Figure 3a and Table S1). Gene ontology analysis revealed that the proteomic profile of the different sEVs is mainly related to pathways involved in cell communication, signal transduction and metabolism (Figure 3b). A quantitative proteomic analysis

shows 65 proteins overrepresented in the chemo-sEVs in comparison with the sEVs derived from the A2780cis (Figure 3c and Table S2). A protein-protein interaction network and functional enrichment analysis of the total proteins found in the chemo-sEVs reveals a network of proteins associated with DNA Double-strand break repair (CHEK2, PRKDC, HIST1H4F, HIST1H2BM, XRCC6, UBA52), proteins of the proteasome complex which are involved in stabilization and regulation of p53, RUNX2 and PTEN (PSMC2, PSMA7, PSMA5, PSMD12, PSMC3, PSMC5, PSMD11, PSMD14, PSMC6, PSMD7 and PSME3), and proteins associated to the metabolism of RNA (mostly ribosomal proteins) (Figure 3d). All these networks have been associated with the acquisition of chemoresistance, therefore this functional network analysis reveals possible mechanisms of how chemo-sEVs could transfer chemoresistance to sensitive cells as we previously described in this work (Figure 2e,f).

### 3.4 | A2780cis cells present a lysosomal alteration phenotype

Further, we investigated the underlying cellular mechanisms that could explain the increased machinery of A2780cis to form MVEs and ILVs, key mediators for the major secretion of chemo-sEVs. In this context, and because of previous findings in C13 cells, other OvCa CDDP-resistant cellular models, suggested that a high number of MVEs could be related with disturbances at the level of lysosomes (Guerra et al., 2019; Safaei et al., 2005), acidic organelles functionally associated with MVEs compartments (Peng et al., 2021), we tested the status of lysosomes between A2780 and A2780cis cells. First, we evaluated by Western blot the protein levels of the structural lysosomal membrane protein LAMP1. Interestingly, we observed a significant decrease in levels of LAMP1 in A2780cis cells compared to A2780 cells (Figure 4a,b). Then, we analyzed by immunofluorescence the number of lysosomes, using as a marker LAMP1 punctated structures stained with Cathepsin D, an acidic luminal hydrolase known as a classical marker of lysosomes (Oberle et al., 2010; Pi et al., 2016). By immunofluorescence we observed that A2780cis showed a notorious decrease in the number of punctated structures positive to both LAMP1 and Cathepsin D (Figure 4c). Quantitative analysis of these images confirmed a significant decrease in the number of LAMP1 (Figure 4d) and Cathepsin D (Figure 4e) structures in the A2780cis cells. Moreover, we found a significant reduction in the average intensity per punctated structure in A2780cis, either positive to LAMP1 (Figure 4f) and Cathepsin D (Figure 4g), compared to A2780 cells. Lysosomes are essential in the regulation of cell proliferation and growth (Shin & Zoncu, 2020). Several cell lines exhibit reduced growth rates and cell viability when grown in media supplemented with FBS EV-depleted (FBS-ED) (Lehrich et al., 2021). To investigate the potential effects of using FBS EV-depleted supplemented medium on sEVs isolation experiments (Figures 2 and 3) and its impact on lysosome phenotypes observed in A2780 and A2780cis cells (Figure 4c–g), we evaluated their phenotype by immunofluorescence. We used LAMP1 and Cathepsin D staining as markers. Our results did not show changes in the levels of LAMP1 and Cathepsin D in A2780 and A2780cis cells cultured in medium supplemented with 5% FBS-ED compared to those supplemented with 10% (Figure S1).

Next, we investigated whether the reduction in LAMP1 and Cathepsin D structures observed in A2780cis cells were indicative of lysosomal function impairment. For this, we performed labeling of acidic compartments with the LysoTracker™-Red probe in live cells (Figure 4h). We observed a significant reduction in the number of acidic structures in A2780cis compared to A2780 (Figure 4i). As observed with LAMP1 and Cathepsin D, the measurement of the average intensity of lysotracker positive structures also showed a significant decrease in A2780cis compared to A2780 cells (Figure 4j). Moreover, because an acidic environment is critical for lysosomal hydrolase activities, we tested whether the reduction in lysosomal acidity in A2780cis cells correlated with a reduction in the activity of the Cathepsin B, an abundant lysosomal hydrolase (Oberle et al., 2010). For this, lysosomes were labeled with the Magic Red®, a probe that allows to quantify the activity of Cathepsin B in live cells (Kundu et al., 2018). As expected, the quantification of average intensity showed a significant reduction in Cathepsin B activity in A2780cis cells with respect to A2780 cells (Figure 4k,l). Finally, considering that RAB7A mediates the trafficking of MVEs and their fusion with lysosomes to the maintenance of this organelle (Bucci et al., 2000), we tested the RAB7 protein in A2780 and A2780cis cells. Surprisingly, and in contrast to our findings with RAB27A (Figure 1i,j), we found that levels of RAB7 were significantly lower in A2780cis compared to A2780 cells (Figure 4m,n). To evaluate a potential relationship between the expression of RAB27A and RAB7, we measured their RNA levels. We observed that RAB27A RNA levels were higher in A2780cis cells than in A2780 cells. Conversely, RAB7 RNA levels were lower in A2780cis cells compared to A2780 cells (Figure 4o). The decrease in RAB7 protein and RNA levels in A2780cis could indicate a reduced fusion capacity of MVEs with lysosomes (Bucci et al., 2000). To evaluate the potential effect of medium supplemented with EV-depleted FBS on the levels of these RABs, we evaluated their protein levels by Western blot. The levels of RAB27A are partially affected in A2780 cells in medium supplemented with 5% FBS-ED compared to cells supplemented with 10% (Figure S2a,c). In A2780cis cells, no significant changes in RAB27A levels were observed between the conditions. Our evidence does not indicate any substantial changes in RAB7 protein levels in both A2780 and A2780cis cells when comparing medium supplemented with 5% FBS-ED to cells supplemented with 10% (Figure S2b,d).

Our findings suggest that the CDDP chemo-resistant phenotype of A2780cis, which is characterized by increased sEVs secretion under CDDP treatment, is likely due to a decline in lysosomal degradative function and a decrease in the levels of RAB7 GTPase levels. This impairs the trafficking and fusion of MVEs towards lysosomes leading to a shift in the trafficking route to the plasma membrane with a subsequent increase in sEVs secretion.

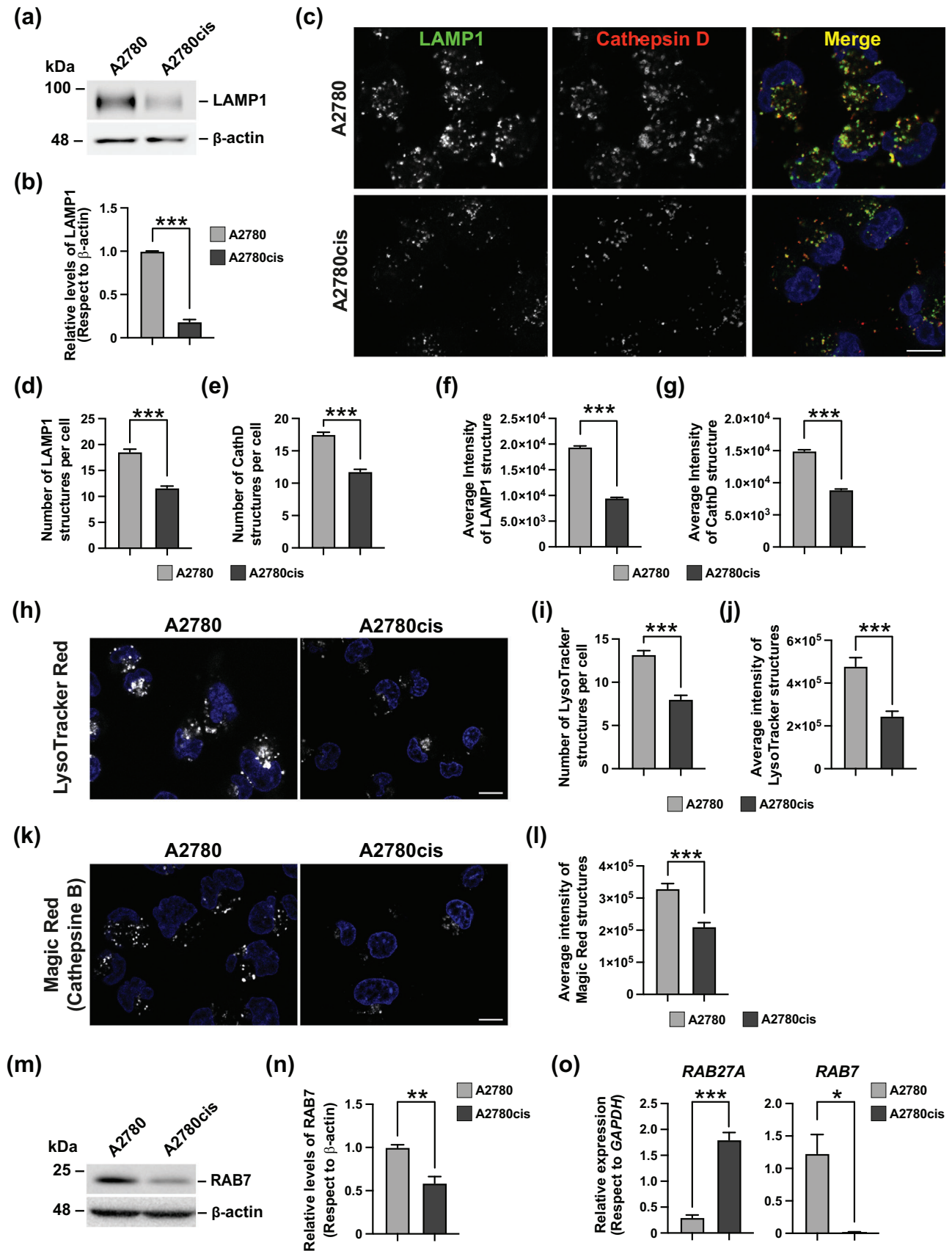


**FIGURE 4** A2780cis CDDP-resistant OvCa cells have lysosomal alteration. (a) Analysis of detergent-soluble protein extracts obtained from A2780 and A2780cis cells by western blot with anti-LAMP1 and anti- $\beta$ -actin. The image is representative of three independent experiments. (b) Densitometric

(Continues)



**FIGURE 4** (Continued)

quantification of the signal of LAMP1 from images as those shown in (a). The signal was normalized with  $\beta$ -actin signal. Bars indicated the mean with SEM; \*\*\* $p < 0.001$ ; one-tiled, paired, non-parametric Mann-Whitney test ( $n = 3$ ). (c) Confocal microscopy images of A2780 and A2780cis PFA-fixed cells immunofluorescent stained with anti-LAMP1 and anti-Cathepsin D. Scale Bar  $10 \mu\text{m}$ . (d,e) Analysis of the number of structures LAMP1 (d) and Cathepsin D (CathD) (e) from images as those shown in (c). Bars indicated the mean with SEM; \*\*\* $p < 0.001$ ; one-tiled, unpaired, parametric  $t$ -test ( $n > 50$  cells). (f,g) Analysis of average intensity of LAMP1 (f) and CathD (g) structures from images as those shown in (c). Bars indicated the mean with SEM; \*\*\* $p < 0.001$ ; one-tiled, unpaired, parametric  $t$ -test ( $n > 50$  cells, from three independent experiments). (h) Confocal live-cell images of A2780 and A2780cis cells incubated with LysoTracker Red and HOECHST33342. Scale Bar  $10 \mu\text{m}$ . (i,j) Analysis of number (i) and average intensity (j) of LysoTracker Red structures from images as those shown in (h). Bars indicated the mean with SEM; \*\*\* $p < 0.001$ ; one-tiled, unpaired, parametric  $t$ -test ( $n > 50$  cells). (k) Confocal live-cell images of A2780 and A2780cis cells incubated with Magic Red and HOECHST33342. Bar  $10 \mu\text{m}$ . (l) Analysis of average intensity of Magic Red structures from images as those shown in (k). Bars indicated the mean with SEM; \*\*\* $p < 0.001$ ; one-tiled, unpaired, parametric  $t$ -test ( $n > 50$  cells, from three independent experiments). (m) Analysis of detergent-soluble protein extracts obtained from A2780 and A2780cis cells by Western blot with anti-RAB7 and anti- $\beta$ -actin. The image is representative of three independent experiments. (n) Densitometric quantification of the signal of RAB7 from images as those shown in (m). The signal was normalized with  $\beta$ -actin signal. Bars indicated the mean with SEM; \*\* $p < 0.01$ ; one-tiled, paired, non-parametric Mann-Whitney test ( $n = 3$ ). (o) Analysis of RAB27A and RAB7 expression concerning GAPDH by qPCR from A2780 and A2780cis cells, with SEM error bar; \*\*\* $p < 0.001$ ; one-tiled non-parametric paired  $t$ -test ( $n = 3$ . Three independent experiments).

### 3.5 | Silencing of RAB27A reduces the secretion of chemo-sEVs from A2780cis cells

The increased secretion of sEVs in A2780cis cells in response to CDDP treatment may be a result of lysosomal dysfunction, as evidenced by the high number of MVEs and ILVs found in these cells which are specialized in secreting of chemo-sEVs in response to CDDP. This phenotype is associated with elevated levels of RAB27A and lower levels of RAB7 (Figure 1i,m-o). It remains unexplored whether the secretion of chemo-sEVs is related to the function of RAB27A and the inverse levels of RAB7 in A2780cis cells. To test this possibility, we silenced RAB27A in A2780cis cells by stable expression of a specific shRNA (shRAB27A). As controls, we generated A2780 and A2780cis cells that stably expressed an shRNA against Luciferase (shLuc). First, we confirmed the efficient silencing of RAB27A in A2780cis cells by Western blot and qPCR (Figure 5a-c). Interestingly, the silencing of RAB27A significantly increased both the protein and transcript levels of RAB7, reaching levels similar to those found in A2780 CDDP-sensitive cells (Figure 5a-c). These findings suggest that RAB27A and RAB7 levels could be interconnected in A2780cis cells.

To evaluate the dependence of chemo-sEVs secretion on RAB27 in A2780cis cells, we isolated sEVs through differential centrifugation from the supernatant media of A2780cis shLuc and A2780cis shRAB27A cells cultured for 72 h (Vera et al., 2019). We also isolated sEVs from both A2780cis shLuc and A2780cis shRAB27A cells treated with  $1 \mu\text{M}$  CDDP for 72 h. NTA analysis revealed that all isolated sEVs were enriched in particles ranging from 100 to 200 nm in diameter (Figure 5d). NTA further showed that treating A2780cis shLuc with CDDP significantly increased the number of secreted sEVs per cell compared to untreated cells, as expected. However, silencing of RAB27A in A2780cis cells did not affect the basal secretion of sEVs per cell compared to control cells (A2780cis shLuc). CDDP treatment in A2780cis shRAB27A cells increased the secretion of sEVs per cell compared to untreated A2780cis shRAB27A cells, but the increase was on a smaller scale than observed for A2780cis shLuc cells (Figure 5e). Our results suggest that RAB27A may regulate the secretion of chemo-sEVs from A2780cis cells.

The recovery of RAB7 levels and the decreased secretion of chemo-sEVs in A2780cis cells following RAB27A silencing suggest that this phenotype could impact their sensibility to CDDP. To investigate this, we measured the Lethal Dose<sub>50</sub> (LD<sub>50</sub>) for CDDP using the Sulforhodamine B (SRB) assay. Cells A2780cis shLuc and A2780cis shRAB27 were treated with different doses of CDDP for 24 h. Our analysis indicates that silencing significantly reduces cell viability upon CDDP treatment (Figure 5f, Two-way ANOVA). In addition, we observed a reduction in LD<sub>50</sub> from  $27.60 \mu\text{M}$  in A2780cis shLuc cells to  $14.69 \mu\text{M}$  in A2780cis shRAB27 cells (Figure 5f).

Quantification of the LD<sub>50</sub> in both cell lines confirmed it decreased by half following RAB27A reduction (Figure 5g). These findings confirm that silencing of RAB27A is a potent strategy to reverse chemo-sEVs secretion and CDDP chemoresistance in OvCa A2780cis cells.

### 3.6 | Silencing of RAB27A restores lysosomal function impairment in A2780cis cells

The silencing of RAB27A leads to a significant increase in RAB7 at both the transcript and protein levels (Figure 5a-c). High levels of RAB7 are usually related typically associated with an increased number of lysosomes (Bucci et al., 2000). To test this possibility, we evaluate the levels of LAMP1 by Western blot. Interestingly, we found that silencing of RAB27A increases the levels of LAMP1 in A2780cis cells, reaching similar levels found in A2780 CDDP sensitive cells (Figure 5a,b). Next, we investigated if the elevated levels of LAMP1 in A2780cis were associated with an increase in the number of lysosomes. By immunofluorescence, we found that silencing of RAB27A in A2780cis led to a marked increase in the number of lysosomes, demonstrated by the increase co-staining of LAMP1 and Cathepsin D (Figure 5c, lower panel compared to the middle panel). Notably, the silencing of

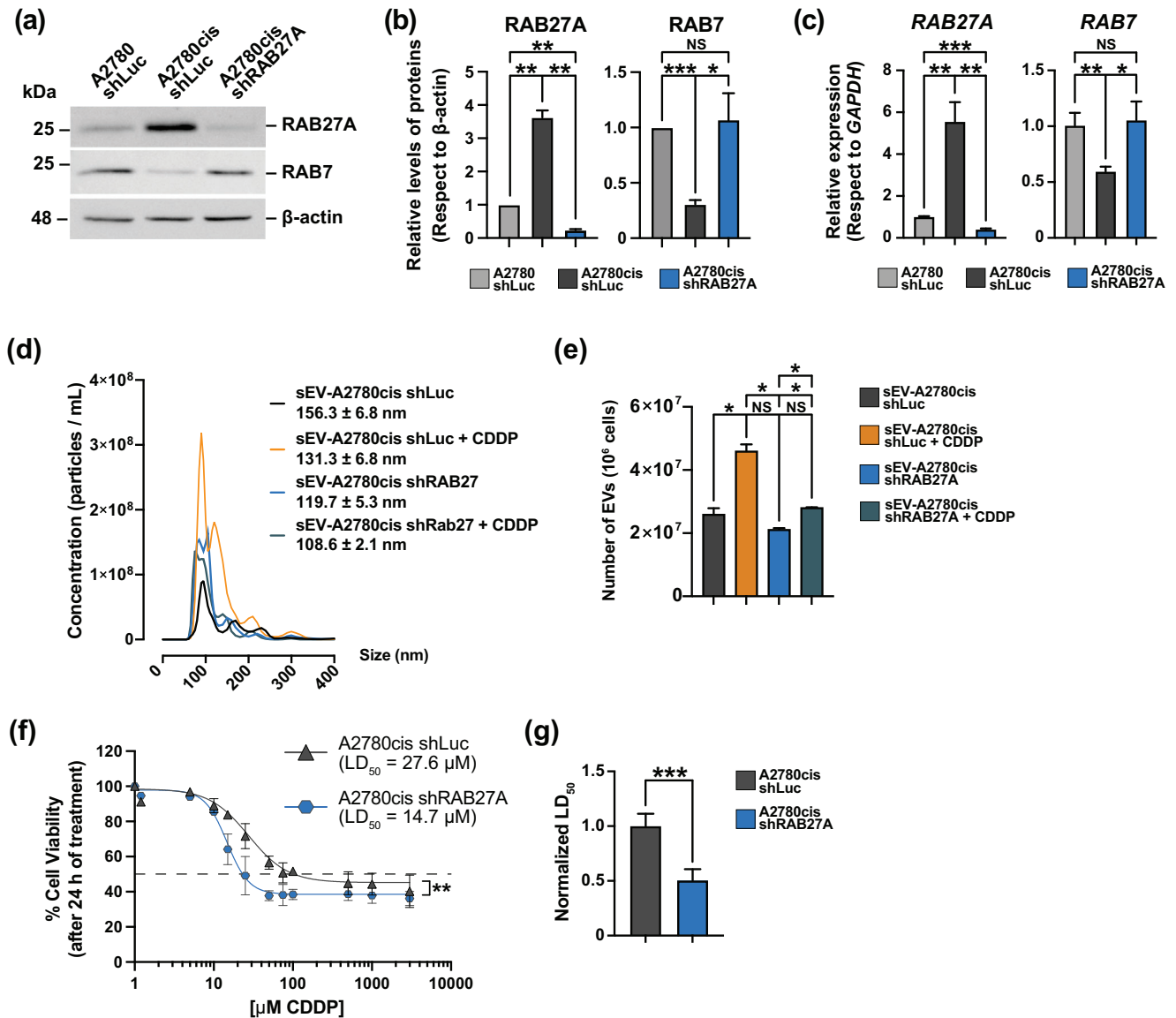


**FIGURE 5** RAB27A silencing expression prevents the secretion of chemo-EVs and sensitizes A2780cis CDDP-resistant to CDDP. (a) Analysis of detergent-soluble protein extracts obtained from A2780 shLuc, A2780cis shLuc and A2780cis shRAB27A stable cell lines by Western blot with anti-RAB27A, anti-RAB7, anti-LAMP1 and  $\beta$ -actin. The image is representative of three independent experiments. (b) Densitometric quantification of the signal of RAB27A, RAB7 and LAMP1 from images as those shown in (a). The signal was normalized with  $\beta$ -actin signal. Bars indicated the mean with SEM; A2780 shLuc samples were normalized to 1 since the biological replicates were run in different Western blot; \* $p < 0.05$ , \*\* $p < 0.01$ , \*\*\* $p < 0.001$ , NS: Not significant; one-tailed, paired, non-parametric Mann-Whitney test ( $n = 3$ ). (c) Analysis of RAB27A and RAB7 expression concerning GAPDH by qPCR from A2780 shLuc, A2780cis shLuc and A2780cis shRAB27A cells, with SEM error bar; \*\*\* $p < 0.001$ ; nonparametric paired  $t$ -test. ( $n = 3$ . Three independent experiments). (d) Nano-tracking analysis (NTA) of sEVs obtained by differential ultracentrifugation (dUC) from 72 h supernatant medium (SM) of A2780cis shLuc (sEVs-A2780 shLuc), A2780cis shLuc cells treated with 1  $\mu$ M CDDP (cisplatin) during 72 h (sEVs-A2780cis shLuc+CDDP), of A2780cis shRAB27A (sEVs-A2780 shRAB27A), A2780cis shRAB27A cells treated with 1  $\mu$ M CDDP (cisplatin) during 72 h (sEVs-A2780cis shRAB27A+CDDP). The quantifications represent the distribution size of the sEVs calculated by the mean concentration of the sEVs of each size ( $n = 3$ . Three independent experiments). (e) Analysis of the number of sEVs-A2780, sEVs-A2780cis and sEVs-A2780cis+CDDP per  $10^6$  cells obtained by dUC. Bars indicated the mean with SEM; \*\* $p < 0.01$ , \*\*\* $p < 0.001$ , NS: not significant; one-tailed, unpaired, non-parametric Man-Whitney test ( $n = 3$ . Three independent experiments). (f) Cell viability percentage curves obtained from the average of biological replicates of A2780cis shLuc and A2780cis shRAB27A treated with increasing doses of CDDP (cisplatin); indicating the comparative analysis of curves by two-way ANOVA, \*\* $p < 0.01$ ; and the general Lethal Dos<sub>50</sub> (LD<sub>50</sub>) to CDDP for each cell. (g) Comparative analysis of LD<sub>50</sub> to CDDP of 2780cis shLuc and A2780cis shRAB27A obtained from each biological replicate, with SEM error bar; \*\*\* $p < 0.001$ ; one-tailed non-parametric paired  $t$ -test.

RAB27A in A2780cis cells facilitated the recovery of lysosomal structures, displaying a pattern similar to A2780 cells (Figure 5c, lower panel compared to the top panel). Quantitative analysis confirmed a significant increase in both the number and average intensity of LAMP1 and Cathepsin D structures per cell (Figure 5d-g). Next, we evaluated if the increase in lysosomal structures was accompanied by enhanced acidity and activity within these organelles. For this, we used the LysoTracker probe, which labels acidic lysosomal compartments. Utilizing the LysoTracker probe, which labels acidic lysosomal compartments, we noted that A2780cis cells showed a significant elevation in the number and intensity of LysoTracker-positive structures with RAB27A silencing, reaching levels comparable to A2780 cells (Figure 5h-j). In addition, silencing of RAB27A in A2780cis cells significantly increased the average intensity of Magic Red labeling, observing similar levels to those found in A2780 cells (Figure 5h,k). Finally, we evaluated levels of the tetraspanin CD63, a protein enriched in MVEs and ILVs, known for its lysosome targeting motif sequence that allows its degradation by lysosomes (Kubo et al., 2017; Mathieu et al., 2021). With the rationale that RAB27A silencing could enhance the trafficking of MVEs towards lysosomal degradation, rather than secretion, led us to examine CD63 levels by immunofluorescence. Surprisingly, we found that silencing of RAB27A in A2780cis cells significantly diminished the number and average intensity of CD63positive structures, similar to the levels observed in A2780 CDDP-sensitive cells (Figure 5l-n). These findings strongly indicate that silencing of RAB27A reverses the altered lysosomal phenotype in A2780cis cells, facilitating the trafficking of MVEs towards lysosomal degradation, rather than secretion, likely similar to the phenotype observed in A2780 CDDP-sensitive cells.

### 3.7 | Reestablishment of lysosomal function in A2780cis cells reduces the secretion of chemo-sEVs and diminishes resistance transfer capacity

Since the silencing of RAB27A may promote the trafficking of MVEs towards a degradative pathway, thereby enhancing lysosomal function and impacting the secretion of chemo-sEVs (Figures 5 and 6), this prompted us to evaluate if another well-known conditions that induces lysosomal activity would result in a similar phenotype. To address this, we tested the effect of rapamycin on A2780cis cells, an inhibitor of the mTORC1 kinase, known as a potent signaling pathway that induces lysosomal function (Palmieri et al., 2011; Settembre et al., 2012). First, we confirmed the inhibitory effect of rapamycin on mTORC1 activity by measuring the phosphorylation of the T389 residue in S6K, known substrate of mTORC1 (Rosner et al., 2012). The effect of rapamycin in A2780cis cells was tested both in the absence and presence of CDDP treatment for 72 h. In line with previous findings, we observed that CDDP treatment enhances mTORC1 activity, as evidenced by an increase in S6K phosphorylation compared to untreated cells (Figure 7a,b) (Gremke et al., 2020). Given that hyperactivation of mTORC1 negatively impacts lysosomal function (Palmieri et al., 2011; Settembre et al., 2012), this supports the hypothesis that the increased secretion of chemo-sEVs by CDDP treatment is due to a decline in lysosomal function. Rapamycin effectively blocked both the basal and CDDP-induced phosphorylation of S6K, as expected (Figure 7a,b). We then investigated whether rapamycin could restore the reduced number of lysosomes observed in A2780cis cells (Figure 4). To this, A2780cis cells treated with rapamycin, both in the absence and presence of CDDP for 72 h, were tested using antibodies against LAMP1 and Cathepsin D (CathD) through immunofluorescence. Rapamycin treatment, either alone or combined CDDP, resulted in an increase in the signal of LAMP1 and Cathepsin D signals in A2780cis cells as demonstrated by immunofluorescence analysis (Figure 7c). In contrast, no changes were observed with CDDP treatment alone, showing a pattern similar to that of untreated cells (Figure 7c). Quantification analysis confirmed a significant increase in the average intensity of structures positive to LAMP1 (Figure 7d) and Cathepsin D (Figure 7e) in the presence of rapamycin. Following, we investigated the effect of rapamycin treatment on the secretion of sEVs by A2780cis cells in response to CDDP treatment (chemo-sEVs) for 72 h. First, we assessed the size distribution of sEVs under each condition using NTA. This analysis showed no changes in size distribution, with sEVs consistently measuring between 130 to 170 nm in diameter across all conditions, confirming their identification as sEVs (Figure 7f). Moreover, we studied the number of sEVs under each condition. Consistent with previous findings, CDDP treatment significantly increases in the secretion of sEVs (Figure 7g). In contrast, rapamycin treatment did not affect the number of sEVs secreted by A2780cis cells, as indicated in Figure 7g. Importantly, rapamycin significantly inhibited the increase in the number of sEVs secreted in response to CDDP, as shown in Figure 7g. The cellular degradation and recycling process called autophagy is controlled by mTORC1, which downregulates ULK1-activating phosphorylations, such as at the S317 residue (Holczer et al., 2020). Autophagy is involved in EV production under conditions of intracellular trafficking alterations (Piletic et al., 2023). We explored whether the effects of CDDP and rapamycin on EV secretion from A2780cis cells could be associated with autophagy activation. We assessed the levels of ULK1 and its phosphorylation at S317. No significant changes were observed in cells treated with CDDP alone. However, rapamycin treatment led to an increase in ULK1 phosphorylation compared to untreated cells, suggesting enhanced autophagy activation. When cells were treated with CDDP, the effects of rapamycin were still noticeable, but to a lesser extent (Figure S3a,b). These findings imply that the reduction in the number of chemo-sEVs mediated by rapamycin, may be linked to the activation of autophagy via ULK1 phosphorylation at S317 residue.

Finally, we studied whether rapamycin could reduce the resistance transfer capacity of sEVs secreted in response to CDDP treatment. Similar to our previous assays, A2780 cells were incubated with 50,000 chemo-sEVs per cell for 16 h. These sEVs were

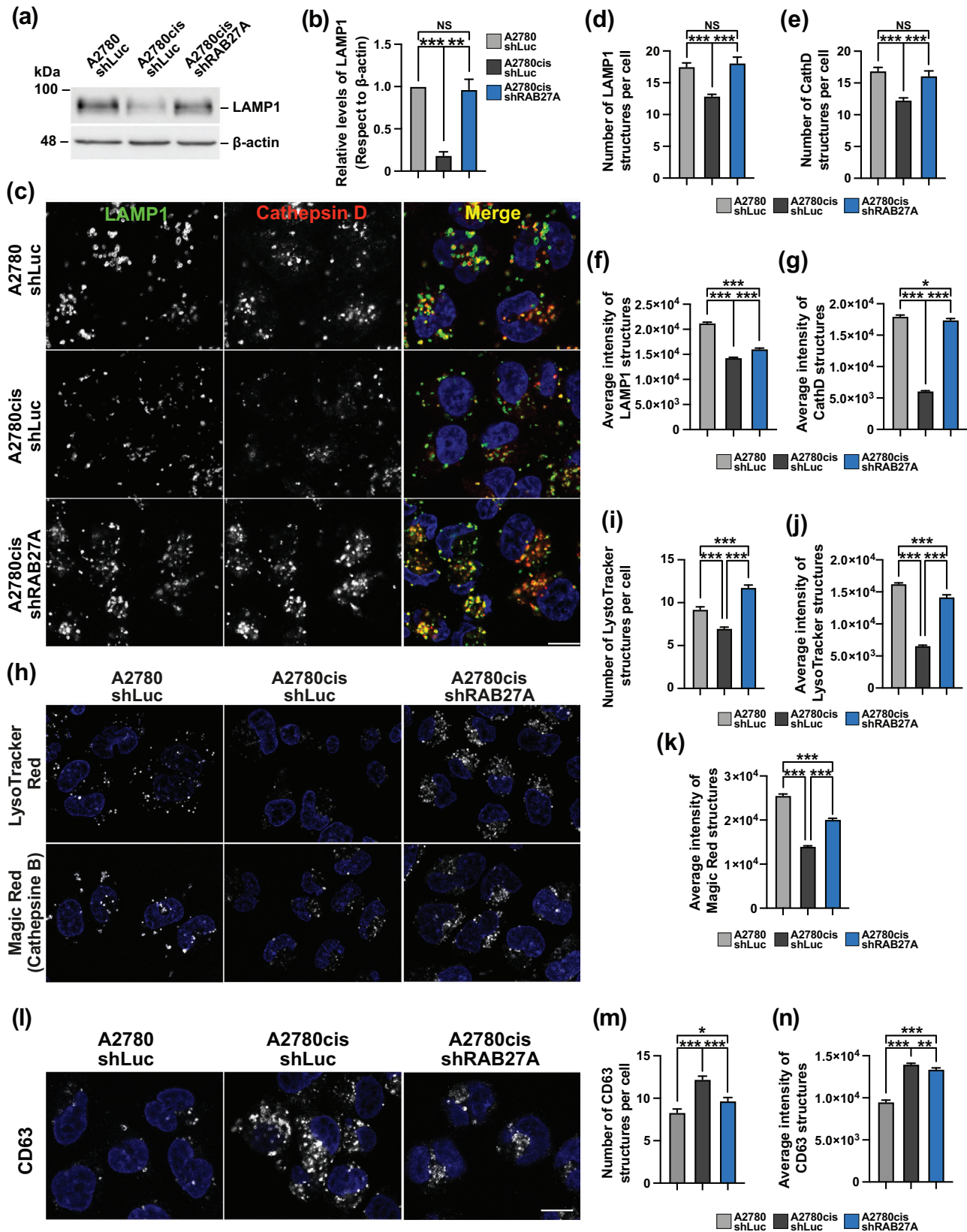


**FIGURE 6** RAB27A silencing expression reverses lysosomal alteration phenotype in A2780cis CDDP-resistant OvCa cells. (a) Analysis of detergent-soluble protein extracts obtained from A2780 shLuc, A2780cis shLuc and A2780cis shRAB27A stable cell lines by Western blot with anti-LAMP1 and  $\beta$ -actin. The image is representative of three independent experiments. (b) Densitometric quantification of the signal of LAMP1 from images as those shown in (a). The signal was normalized with  $\beta$ -actin signal. Bars indicated the mean with SEM; A2780 shLuc samples were normalized to 1 since the biological replicates were run in different Western blot; \* $p < 0.05$ , \*\* $p < 0.01$ , \*\*\* $p < 0.001$ , NS: not significant; one-tailed, paired, non-parametric Mann-Whitney test ( $n = 3$ ). (c)

(Continues)



**FIGURE 6** (Continued)

Confocal microscopy images of A2780 shLuc, A2780cis shLuc and A2780cis shRAB27A PFA-fixed cells immunofluorescent stained with anti-LAMP1 and anti-Cathepsin D. Scale Bar 10  $\mu\text{m}$ . (d,e) Analysis of the number of structures of LAMP1 (d) and Cathepsin D (CathD) (e) from images as those shown in (c). Bars indicated the mean with SEM; \*\*\* $p < 0.001$ , NS: not significant; one-tiled unpaired  $t$ -test ( $n > 50$  cells). (f,g) Analysis of average intensity of LAMP1 (f) and CathD (g) structures from images as those shown in (c). Bars indicated the mean with SEM; \* $p < 0.05$ , \*\*\* $p < 0.001$ ; one-tiled, unpaired, parametric  $t$ -test ( $N > 50$  cells). (h) Confocal live cell images of A2780 shLuc, A2780cis shLuc and A2780cis shRAB27A cells were incubated with LysoTracker Red and HOECHST or Magic Red and HOECHST33342. Scale Bar 10  $\mu\text{m}$ . (i,j) Analysis of number (i) and average intensity (j) of LysoTracker Red structures from images as those shown in (h). Bars indicated the mean with SEM; \*\*\* $p < 0.001$ ; one-tiled, unpaired, parametric  $t$ -test ( $n > 50$  cells from three independent experiments). (k) Analysis of average intensity of Magic Red structures from images as those shown in (h). Bars indicated the mean with SEM; \*\*\* $p < 0.001$ ; one-tiled, unpaired, parametric,  $t$ -test ( $n > 50$  cells from three independent experiments). (l) Confocal microscopy images of A2780 shLuc, A2780cis shLuc and A2780cis shRAB27A PFA-fixed cells immunofluorescent stained with anti-CD63. (m,n) Analysis of number (i) and average intensity (j) of CD63 per cell from images as those shown in (h). Bars indicated the mean with SEM; \* $p < 0.05$ , \*\* $p < 0.01$ , \*\*\* $p < 0.001$ ; one-tiled, unpaired, parametric  $t$ -test ( $n > 50$  cells).

isolated from the supernatant medium of A2780cis cells treated for 72 h under each condition. Following incubation with chemo-sEVs, A2780 cells were treated with 3  $\mu\text{M}$  CDDP for 48 h, and live/dead cells were measured by flow cytometry and trypan blue staining. As expected, we observed 3  $\mu\text{M}$  CDDP caused a mortality rate of 50% of mortality in A2780 cells not treated with sEVs (non-sEVs) (Figure 7h,i). Consistent to our previous findings, the sEVs fraction isolated in the presence of CDDP (chemo-sEVs) conferred resistance to CDDP-induced cell death in A2780 cells (Figure 7h,i). Importantly, this cell death resistance phenotype was reverted when A2780 cells were incubated with in the presence of sEVs isolated in the presence of CDDP and rapamycin (Figure 7h,i). Our findings indicate that the transfer of chemo-resistance to A2780 chemo-sensitive cells by chemo-sEVs secreted by A2780cis cells can be mitigated by enhancing lysosomal function through the inhibition of mTORC1 by rapamycin.

## 4 | DISCUSSION

Chemo-sEVs in OvCa are key players in the acquisition and transference of CDDP-chemoresistance (Safaei et al., 2005; Xavier et al., 2022; Yáñez-Mó et al., 2015). Therefore, the design of new strategies against OvCa and the development of chemoresistance to CDDP requires a deep understanding of the mechanisms related to the role of these sEVs in this type of cancer. In general, the type and quantity of EVs are controlled intracellularly through its biogenesis at the level of MVEs and ILVs and/or with the trafficking and fusion of MVEs with the PM (Dixon et al., 2023; Steinbichler et al., 2019; van Niel et al., 2018). In this work, we revealed that the A2780cis a cellular model of OvCa, that develops chemoresistance to CDDP, exhibits an increased size of MVEs and an increased number of ILVs. This conclusion is based on the analysis of C63 structures (Vanlandingham & Ceresa, 2009; White et al., 2006) and evidence from electronic microscopy. Consistent with this, A2780cis cells have high levels of ESCRTs and RAB27A proteins, which mediate ILVs biogenesis and secretion in A2780cis cells. Interestingly, there are transcriptional and post-translational pathways that could explain this phenotype. For example, the NF- $\kappa\text{B}$  pathway increases the expression of RAB27A through RelA-p60, a mechanism that has been involved in CDDP chemoresistance in bladder cancer (Kan et al., 2020; Liu et al., 2017), however, it is unknown whether this mechanism could explain the RAB27A levels in A2780cis cells or in OvCa models. Additionally, the transcription factor EGFR, which controls RAB27A expression in other cellular models, is overexpressed in A2780cis cells (Ma et al., 2020; Rouillard et al., 2016). Moreover, high levels of RAB27A protein could also be the result of an increased protein stability related to its interaction with KIBRA, a scaffold protein involved in membrane trafficking such as the transport of early endosomes (Traer et al., 2007) in MVEs, which prevents RAB27A proteasomal degradation (Song et al., 2019). Although the link between CDDP and ESCRTs has been less investigated, it is known that CDDP promotes the activation of EGFR (Benhar et al., 2002), a growth factor known to induce the biogenesis of ILVs and the recruitment of ESCRTs to MVEs (Quinney et al., 2019). Altogether, these antecedents suggest that chemoresistance to CDPP in A2780cis cells might be the result of the activation in all these types of pathways, aspects that need further exploration.

Several RAB GTPases play a crucial role in the control of the trafficking of MVEs (Zerial & McBride, 2001). Among all RABs, we discovered that A2780cis cells have higher protein and transcriptional levels of RAB27A compared to A2780 cells (Figures 1i,j and 4o). In this regard, we propose that the acquisition of CDDP resistance is the result of adaptive tumoural cellular processes related to the biogenesis of ILVs and their secretion due to the overexpression of ESCRT machinery and the accessory protein ALIX (Figure 1g,h) and RAB27A (Figure 1i,j). Previous studies suggested that the C13 CDDP-resistant model of OvCa cells secreted more EVs than its sensitive counterpart cellular model (Safaei et al., 2005). However, we did not observe a difference in the basal secretion of sEVs when we compared A2780 and A2780cis cell lines, observing only an increase when A2780cis cells were treated with CDDP, corresponding to chemo-sEVs (Figure 2). Different post-translational modifications (PTMs) regulate the localization and function of different RABs, including phosphorylation, palmitoylation and ubiquitination, among others (Homma et al., 2021; Shinde & Maddika, 2018). Based on previous reports (Kielbik et al., 2018; Nguyen et al., 2017; Shi et al., 2021) CDDP could induce PTMs on RAB27A or in its effectors, causing the activation of RAB27A to promote chemo-sEVs secretion. In the tumour microenvironment, the chemoresistant cell population can spread its resistance mechanisms to remnant-sensitive cells (Madden et al., 2020; Yang et al., 2020). Interestingly, our results indicate that chemo-sEVs secreted in response to CDDP

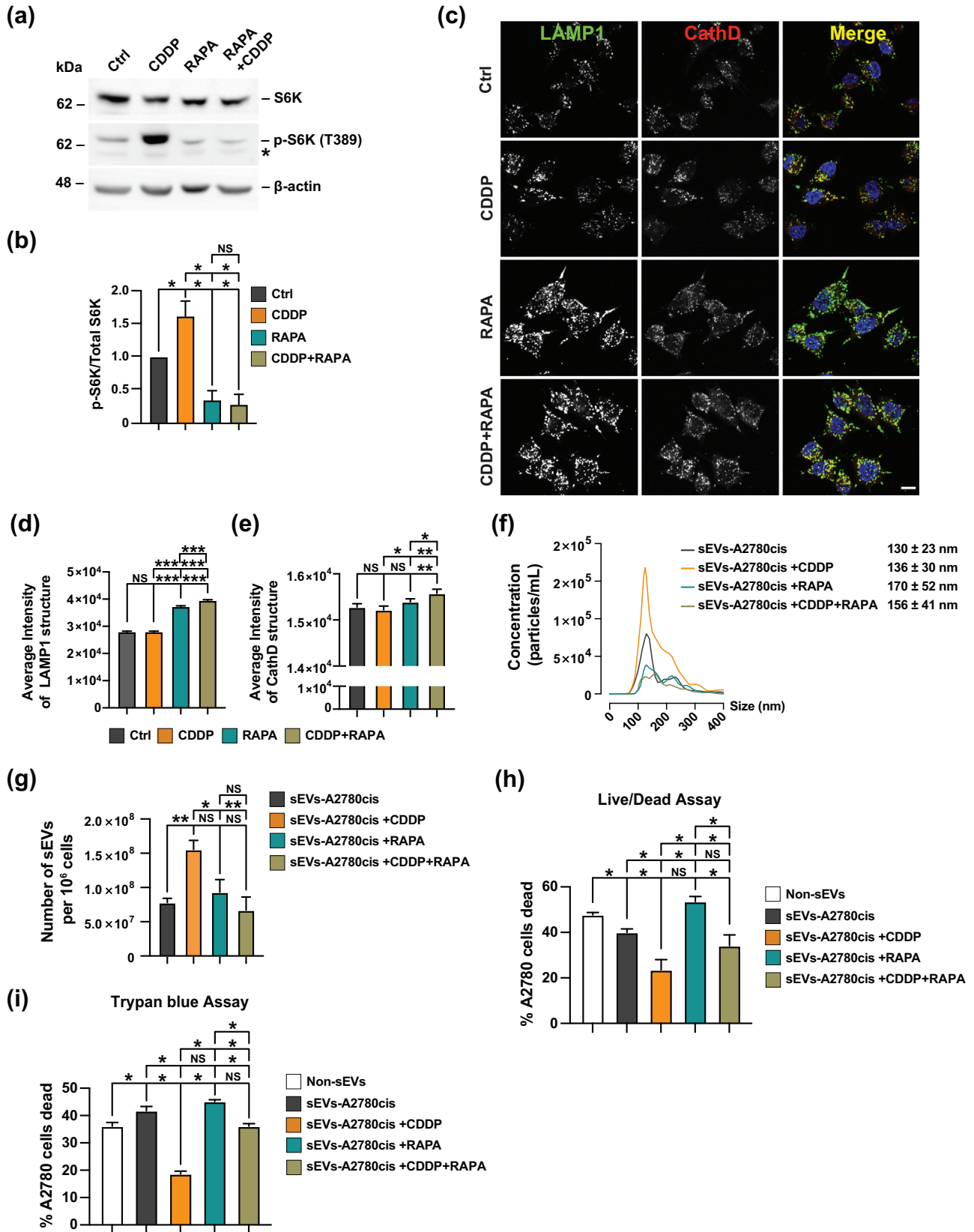


**FIGURE 7** Induction of lysosomal biogenesis by rapamycin prevents CDDP effect on A2780cis CDDP-resistant OvCa cells in the secretion of sEVs and chemoresistance transference capacity. (a) Analysis of detergent-soluble protein extracts obtained from A2780cis control, treated with 1  $\mu$ M CDDP, 100 nM rapamycin (RAPA) or 1  $\mu$ M CDDP (Cisplatin) plus 100 nM RAPA (rapamycin) during 72 h, by Western blot with anti-S6K, anti-S6K (T389) and  $\beta$ -actin. (b) Densitometric quantification of the signal of p-S6K (T389) with respect to total S6K. Bars indicated the mean with SEM; Control samples were normalized to 1 since the biological replicates were run in different Western blot; \* $p < 0.05$ , NS: not significant; one-tiled, paired, non-parametric Mann-Whitney test ( $n = 3$ ).

(Continues)

**FIGURE 7** (Continued)

Three independent experiments). (c) Confocal microscopy images of A2780cis control, treated with 1  $\mu$ M CDDP, 100 nM RAPA or 1  $\mu$ M CDDP plus 100 nM RAPA during 72 h. PFA-fixed cells immunofluorescent stained with anti-LAMP1 and anti-Cathepsin D. Scale Bar 10  $\mu$ m. (d,e) Analysis of average intensity of structures of LAMP1 (d) and CathD per cell (e) from images as those shown in (c). Bars indicated the mean with SEM; \* $p$  < 0.05, \*\* $p$  < 0.01, \*\*\* $p$  < 0.001, NS: not significant; one-tiled, unpaired, parametric *t*-test ( $n$  > 50 cells, from three independent experiments). (f) NTA of sEVs obtained by dUC from 72 h CM of A2780cis (sEVs-A2780cis), A2780cis cells treated with 1  $\mu$ M CDDP during 72 h (sEVs-A2780cis+CDDP), treated with 100 nM RAPA during 72 h (sEVs-A2780cis+RAPA), and treated with 1  $\mu$ M CDDP plus 100 nM RAPA during 72 h (sEVs-A2780cis+CDDP+RAPA). The quantifications represent the distribution size of the sEVs calculated by the mean concentration of the sEVs of each size ( $n$  = 5). (g) Analysis of the number of sEVs-A2780cis, sEVs-A2780cis+CDDP, sEVs-A2780cis+RAPA and sEVs-A2780cis+CDDP+RAPA per 10<sup>6</sup> cells of obtained by dUC. Bars indicated the mean with SEM; \* $p$  < 0.05, \*\* $p$  < 0.01, NS: not significant; one-tiled, unpaired, non-parametric Mann-Whitney test ( $n$  = 5. Five independent experiments). (h,i) Live/Dead cell stain analysis by flow cytometry (h) and trypan blue analysis (i) of A2780 cells treated with 3  $\mu$ M CDDP for 48 h after 16 h of stimulation with PBS (Non-sEVs) or with sEVs-A2780cis, sEVs-A2780cis+CDDP, sEVs-A2780cis+RAPA or sEVs-A2780cis+CDDP+RAPA obtained by dUC. The analysis represents the percentage of A2780 cells dead for each condition. Bars indicated the mean with SEM; \* $p$  < 0.05, NS: not significant; one-tiled, paired, non-parametric Mann-Whitney test ( $n$  = 3. Three independent experiments).

in A2780cis cells (Figure 2d), act as a mediator of cell-cell communication, transferring to A2780 cell the ability to evade CDDP-induced cell death (Figure 2e,f). The cell-cell communication supported by sEVs is associated with the transference of messenger RNAs (mRNAs), miRNAs, DNAs, lipids and proteins (Steinbichler et al., 2019). Our proteomic analysis shows that CDDP changes the content of chemo-sEVs (Figure 3a,c), whereas many of the differentially overrepresented proteins found could contribute to the transfer of chemoresistance to sensitive cells. For example, CHEK2 (Chk2) is a protein involved in DNA repair which is activated when DNA undergoes double strand break (DSB), promoting the arrest of the cell cycle (van Jaarsveld et al., 2020; Zhang et al., 2004). Similarly, we found XRCC6 (Ku70) and PRKDC, proteins involved in DSB repair by non-homologous end joining (Chen et al., 2021; Yu et al., 2018). Since CDDP induces DSB (Sears & Turchi, 2012; Wang et al., 2018), the transfer of these proteins by chemo-sEVs in response to CDDP could promote an activation of the DNA Damage response (DDR) in the recipient cells increasing its capacity to repair DNA, and therefore protecting sensitive cells against the DNA damage produced by CDDP. Supporting this idea, it has been reported that exosomes isolated from bone marrow mesenchymal stem cells (exoBM-MSCs) accelerated the DNA damage repair of recipient BM-MSCs treated with radiation, reducing the deleterious effect of this treatment (Zuo et al., 2020). Stabilization of p53 also plays an important role in DNA repair participating in the arrest of the cell cycle, thus giving time to the DNA repair machinery to facilitate genome stability (Williams & Schumacher, 2016). p53 is stabilized by the ubiquitination-deubiquitination cycle (Lee & Gu, 2010; Li et al., 2002). In this context, we observed that several proteins found enriched in the chemo-sEVs could be implicated in the balance between ubiquitination and deubiquitination of p53 (Figure 3d). For example, the proteasomal deubiquitinase PSMD14, together with PSMD7 as a heterodimer, promotes p53 protein stability through a non-canonical pathway independent of the catalytic barrel of the 20S proteasome, function recently implicated in cancer progression (Bustamante et al., 2023). Interestingly, we found an enrichment of PSMD14 and PSMD7 in the chemo-sEVs isolated from A2780cis cells in response to CDDP. Therefore, it could be interesting to explore if this proteasome heterodimer could promote the stabilization of p53 in the recipient sensitive A2780 cells. Other possible proteins implicated could be related to the metabolism of the RNA such as ribosomal proteins (RPs), which have been suggested to play a role in drug resistance and cancer progression (Avitabile et al., 2022; Huang et al., 2020; Kobayashi et al., 2006; Liu et al., 2019; Zhao et al., 2021). In fact, it has been reported in a model of CDDP-resistant gastric cancer that exosomes derived from these cells transfer chemoresistance to their sensitive counterparts via exosomal RPS3 (Sun et al., 2021). In this context, we found an enrichment of several RPs proteins, including RPS3, in the chemo-sEVs isolated from A2780cis cells in response to CDDP treatment (Figure 3d). The mechanism underlying the observed cargo selection requires further investigation in future research. Our characterization of sEVs isolation revealed an increase in Syntenin-containing sEVs obtained from A2780cis cells treated with CDDP. Syntenin is known as a cargo selector in the Syndecan-Syntenin-ALIX pathway, which is crucial for ILVs/exosome biogenesis (Baietti et al., 2012; Leblanc et al., 2020). Further investigation will help to define the more determinant players responsible for chemoresistance in sensitive cells. Proteomic analysis of chemo-sEVs presents a valuable strategy to gain insights into these processes. However, the next challenge is to demonstrate which of these components contribute to cancer progression during chemotherapy.

In this study, we have underscored a fine regulatory mechanism that controls the secretion of chemo-sEVs related to a step that defines the fusion of MVEs with the PM for secretion or alternatively with lysosomes for degradation, where the molecular details that exactly define one or another direction are only partially understood (Huotari & Helenius, 2011; van Niel et al., 2018). Recently, it has been reported that the exchange between RAB7 and RAB27A on MVEs that controls exosome secretion is modulated by the ER membrane contact sites with endosomes (Verweij et al., 2022), opening a new hypothesis about how the secretion of chemo-sEVs is regulated. In this context, the levels of RAB27 and RAB7 in A2780cis cells seem to be mutually regulated, whereas upregulation of RAB27A correlates with a downregulation of RAB7, a phenotype that promotes the secretion of chemo-sEVs in response to CDDP (Figures 1i,j and 4m,o). Interestingly, hypoxia has been shown to trigger a similar phenotype regarding the balance of RAB27A/RAB7, a condition that also promotes an increased secretion of exosomes in chemoresistant ovarian cancer (Dorayappan et al., 2018). Regarding these findings, it is interesting the hypothesis that claims that the trafficking of MVEs is regulated by a fine balance between the status of lysosomal function and the cellular capacity for exosomal secretion

(Eitan et al., 2016; Xu et al., 2022). Surprisingly, A2780cis showed a reduced number of lysosomes, and the remaining lysosomes present low acidity, compromising their degradative function (Figure 4a-l). In agreement with previous findings (Kalayda et al., 2008; Safaei et al., 2005), we propose that the decay in lysosomal function together with an increase in key proteins needed for secretion, such as RAB27A, is mandatory to promote the biogenesis of MVEs and secretion of ILVs in response to CDDP in A2780cis cells (Figure 2d), initial events in the development of chemoresistance. Additionally, the downregulation of RAB7 (Figure 4m-o) might act as a key step to initiate the dysfunction of the lysosomal pathway in response to CDDP, an event that could decrease the delivery of hydrolases or proteins needed for pH maintenance (Saftig & Klumperman, 2009; Trivedi et al., 2020; Yang & Wang, 2021). In this context, it will be interesting to explore the impact of CDDP in the levels of those accessory proteins of AP-1 and GGAs complexes implicated in the delivery of hydrolases to lysosomes such as p56 (Mardones et al., 2007) and cyclin G-associated kinase (GAK) (Kametaka et al., 2007), among several others.

On the other hand, lysosomes have a drug-sequestering function that diminishes the availability of the drugs within cells including CDDP (Galluzzi et al., 2014; Geisslinger et al., 2020; Zhai & Hiani, 2020; Zhitomirsky & Assaraf, 2016). Thus, the process of chemotherapy resistance may be driven by the sequestration of CDDP within lysosomes (Galluzzi et al., 2014; Geisslinger et al., 2020; Zhai & Hiani, 2020; Zhitomirsky & Assaraf, 2016), leading to lysosomal dysfunction observed in A2780cis cells during the early stages of resistance acquisition (Figure 4). This sequestration can cause the secretion of sEVs that can become more pronounced over time due to high levels of RAB27A, resulting in the orchestration of a cell survival program and the development of chemotherapy resistance. Thus, in addition to the mechanism described for chemoresistance to CDDP (Chen & Chang, 2019), we propose RAB27A-dependent chemo-sEVs secretion is a novel pathway activated under lysosomal dysfunction and a critical feature for CDDP chemoresistance in OvCa. Future experiments should address the process of CDDP sequestration in lysosomes during the acquisition of resistance and changes in its degradative function.

In addition to the direct role of the CDDP in lysosomes, it is possible that CDDP could activate a signaling pathway with a negative impact on lysosomes. In this regard, it has been demonstrated that CDDP activates mTORC1 causing the inactivation of the transcription factor TFE3 (O'Dea et al., 1988; Palmieri et al., 2011). Consistently, CDDP treatment in A2780cis cells leads to the activation of mTORC1 (Figure 7a,b), a response that may underlie lysosomal dysfunction (Fang et al., 2022), which should be further investigated. Additionally, A2780cis cells show reduced protein and transcriptional levels of the RAB7, suggesting the involvement of this GTPase in the decline of the lysosomal function during the acquisition of chemoresistance.

Importantly, the silencing of RAB27A in A2780cis cells, a strategy that inhibits the secretion of exosomes in a variety of other cellular models (Blanc & Vidal, 2018; Bobrie et al., 2012; Huang et al., 2021; Ostrowski et al., 2010; Salimu et al., 2017), promotes an increase in the protein levels of RAB7, confirming a closed regulation between these two GTPases. Moreover, silencing of RAB27A also causes a recovery in the number and function of lysosomes, together with a decrease in CD63 strongly indicates that silencing of RAB27A enhances the delivery of content into the endo-lysosomal degradative pathway. Further studies should be addressed if overexpression of RAB7 could be sufficient to recapitulate the effect observed with the silencing of RAB27. Moreover, we found that inhibition of mTORC1 with rapamycin, a well-known strategy to promote lysosomal biogenesis, affects the secretion of chemo-sEVs in A2780cis cells in response to CDDP. Moreover, the chemo-sEVs secreted have a reduced capacity to transfer chemoresistance in sensitive cells. Altogether, these findings confirm a close interplay between the lysosomal function and the capacity of cells to secrete chemo-sEVs, in which the interruption of one pathway impacts positively the other.

These findings offer possible targets of intervention for OvCa patients that develop chemoresistance to CDDP including drugs with a potent inhibitory effect on sEVs secretion such as specific inhibitors of RAB27A activity (Zhang et al., 2020). Another strategy could be related to an induction of the lysosomal function through the biogenesis of these organelles with the use of rapamycin, a compound that enhances the anti-tumoural effects of derivatives of CDDP (oxaliplatin) in A2780cis (Liu et al., 2015). Moreover, high levels of RAB7 in the C13 CDDP-resistant model of OvCa cells have been demonstrated to sensitize cells to CDDP (Guerra et al., 2019), which based on our results could be due to an increase in the degradative endo-lysosomal pathway and lysosome biogenesis.

The results of this study provide insight into the development of CDDP chemoresistance in OvCa. By uncovering the interplay between lysosomal function and the secretion of chemo-sEVs, two new potential strategies against CDDP chemoresistance were identified: silencing of RAB27A and inhibition of mTORC1 with rapamycin. These interventions aim to revert the lysosomal dysfunction found in CDDP-resistant cancer cells and may improve the efficiency of CDDP-based cancer treatments. The findings of this study have the potential to improve the design of complementary strategies incorporating lysosomal-targeting agents to overcome CDDP chemoresistance.

## AUTHOR CONTRIBUTIONS

**Cristóbal Cerda-Troncoso:** Conceptualization; data curation; formal analysis; investigation; methodology; project administration; software; supervision; validation; visualization; writing—original draft; writing—review and editing. **Felipe Grünenwald:** Data curation; formal analysis; validation. **Eloísa Arias-Muñoz:** Data curation; formal analysis; software; visualization; writing—review and editing. **Viviana A. Cavieres:** Formal analysis; funding acquisition; methodology; software; visualization; writing—review and editing. **Albano Caceres-Verschae:** Formal analysis; methodology; supervision; validation; writing—review and editing. **Belén Gaete-Ramírez:** Data curation; formal analysis; methodology; resources; software; writing—review



and editing. **Francisca Álvarez-Astudillo:** Data curation; formal analysis; funding acquisition; methodology; visualization; writing—review and editing. **Rodrigo A. Acuña:** Methodology; visualization; writing—review and editing. **Matias Ostrowski:** Conceptualization; formal analysis; resources; supervision; writing—review and editing. **Patricia V. Burgos:** Conceptualization; data curation; formal analysis; funding acquisition; investigation; methodology; project administration; resources; software; supervision; validation; visualization; writing—original draft; writing—review and editing. **Manuel Varas-Godoy:** Conceptualization; data curation; formal analysis; funding acquisition; investigation; methodology; project administration; resources; software; supervision; validation; visualization; writing—original draft; writing—review and editing.

## ACKNOWLEDGEMENTS

We thank Dr Sarah Reed and Dr Buddhika Jayakody from the mass spectrometry facility of the University of Queensland Centre for Clinical Research (UQCCR) for their technical support during mass spec experiments. We also thank Dr Ana L. Riveros Salvatierra (FONDEQUIP EQM160157, School of Chemical and Pharmaceutical Sciences, University of Chile) for her technical assistance in particle analysis determination. The main research was performed in the Doctoral Thesis of Dr Cristóbal Cerda-Troncoso titled ‘Decoding adaptive cellular mechanisms of cisplatin chemoresistance in ovarian cancer cells’, presented in April of 2022 (Cerda-Troncoso, 2022). This research was funded by Fondo Nacional de Desarrollo Científico y Tecnológico de Chile (FONDECYT) grants numbers 1171649 and 1211261 (Patricia V. Burgos), 1190928 and 1230983 (Manuel Varas-Godoy); ANID/BASAL/FB210008 (Manuel Varas-Godoy and Patricia V. Burgos); FONDECYT postdoctoral fellowship 3220485 (Viviana A. Cavieres) 3200825 (Francisca Álvarez-Astudillo) and; Fondo de Financiamiento de Centros de Investigación en Áreas Prioritarias (FONDAP) grant 15130011 (Manuel Varas-Godoy); ANID doctoral fellowship 21230341 (Belén Gaete-Ramírez); and Vicerrectoría de Investigación y Doctorados, Universidad San Sebastián for PhD scholarship (Cristóbal Cerda-Troncoso).

## CONFLICT OF INTEREST STATEMENT

The authors declare that the research was conducted in the absence of any commercial or financial relationships that could be construed as a potential conflict of interest.

## ORCID

Cristóbal Cerda-Troncoso  <https://orcid.org/0000-0002-7573-1997>

Patricia V. Burgos  <https://orcid.org/0000-0003-4521-7978>

Manuel Varas-Godoy  <https://orcid.org/0000-0001-5857-4793>

## REFERENCES

- Ab Razak, N. S., Ab Mutalib, N. S., Mohtar, M. A., & Abu, N. (2019). Impact of chemotherapy on extracellular vesicles: Understanding the chemo-EVs. *Frontiers in Oncology*, 9, 1113. <https://doi.org/10.3389/fonc.2019.01113>
- Adams, S. D., Csere, J., D’angelo, G., Carter, E. P., Romao, M., Armandis, T., Dodel, M., Kocher, H. M., Grose, R., Raposo, G., Mardakheh, F., & Godinho, S. A. (2021). Centrosome amplification mediates small extracellular vesicle secretion via lysosome disruption. *Current Biology: CB*, 31(7), 1403–1416.e7.
- Ai, Z., Lu, Y., Qiu, S., & Fan, Z. (2016). Overcoming cisplatin resistance of ovarian cancer cells by targeting HIF-1-regulated cancer metabolism. *Cancer Letters*, 373(1), 36–44. <https://doi.org/10.1016/j.canlet.2016.01.009>
- Alharbi, M., Lai, A., Sharma, S., Kalita-de Croft, P., Godbole, N., Campos, A., Guanzon, D., Salas-Burgos, A., Carrion, F., Zuñiga, F. A., Perrin, L., He, Y., Pejovic, T., Winters, C., Morgan, T., Hooper, J. D., Rice, G. E., & Salomon, C. (2021). Extracellular vesicle transmission of chemoresistance to ovarian cancer cells is associated with hypoxia-induced expression of glycolytic pathway proteins, and prediction of epithelial ovarian cancer disease recurrence. *Cancers*, 13(14), 3388. <https://doi.org/10.3390/cancers13143388>
- Altick, A. L., Baryshnikova, L. M., Vu, T. Q., & von Bartheld, C. S. (2009). Quantitative analysis of multivesicular bodies (MVBs) in the hypoglossal nerve: Evidence that neurotrophic factors do not use MVBs for retrograde axonal transport. *The Journal of Comparative Neurology*, 514(6), 641–657. <https://doi.org/10.1002/cne.22047>
- Andreu, Z., & Yáñez-Mó, M. (2014). Tetraspanins in extracellular vesicle formation and function. *Frontiers in Immunology*, 5, 1–12. <https://doi.org/10.3389/fimmu.2014.00442>
- Avitabile, M., Bonfiglio, F., Aievola, V., Cantalupo, S., Maiorino, T., Lasorsa, V. A., Domenicotti, C., Marengo, B., Zbyněk, H., Vojtěch, A., Iolascon, A., & Capasso, M. (2022). Single-cell transcriptomics of neuroblastoma identifies chemoresistance-associated genes and pathways. *Computational and Structural Biotechnology Journal*, 20, 4437–4445. <https://doi.org/10.1016/j.csbj.2022.08.031>
- Bae, D., Moore, K. A., Mella, J. M., Hayashi, S. Y., & Hollien, J. (2019). Degradation of *Blos1* mRNA by IRE1 repositions lysosomes and protects cells from stress. *The Journal of Cell Biology*, 218(4), 1118–1127. <https://doi.org/10.1083/jcb.201809027>
- Baietti, M. F., Zhang, Z., Mortier, E., Melchior, A., Degeest, G., Geeraerts, A., Ivarsson, Y., Depoortere, F., Coomans, C., Vermeiren, E., Zimmermann, P., & David, G. (2012). Syndecan-syntenin-ALIX regulates the biogenesis of exosomes. *Nature Cell Biology*, 14(7), 677–685. <https://doi.org/10.1038/ncb2502>
- Bandari, S. K., Purushothaman, A., Ramani, V. C., Brinkley, G. J., Chandrashekar, D. S., Varambally, S., Mobley, J. A., Zhang, Y., Brown, E. E., Vlodaysky, I., & Sanderson, R. D. (2018). Chemotherapy induces secretion of exosomes loaded with heparanase that degrades extracellular matrix and impacts tumor and host cell behavior. *Matrix Biology: Journal of the International Society for Matrix Biology*, 65, 104–118. <https://doi.org/10.1016/j.matbio.2017.09.001>
- Bandari, S. K., Tripathi, K., Rangarajan, S., & Sanderson, R. D. (2020). Therapy-induced chemoexosomes: Sinister small extracellular vesicles that support tumor survival and progression. *Cancer Letters*, 493, 113–119. <https://doi.org/10.1016/j.canlet.2020.08.022>
- Benhar, M., Engelberg, D., & Levitzki, A. (2002). Cisplatin-induced activation of the EGF receptor. *Oncogene*, 21(57), 8723–8731. <https://doi.org/10.1038/sj.onc.1205980>

- Blanc, L., & Vidal, M. (2018). New insights into the function of Rab GTPases in the context of exosomal secretion. *Small GTPases*, 9(1-2), 95–106. <https://doi.org/10.1080/21541248.2016.1264352>
- Bobrie, A., Krumeich, S., Reyat, F., Recchi, C., Moita, L. F., Seabra, M. C., Ostrowski, M., & Théry, C. (2012). Rab27a supports exosome-dependent and -independent mechanisms that modify the tumor microenvironment and can promote tumor progression. *Cancer Research*, 72(19), 4920–4930. <https://doi.org/10.1158/0008-5472.CAN-12-0925>
- Bolte, S., & Cordelières, F. P. (2006). A guided tour into subcellular colocalization analysis in light microscopy. *Journal of Microscopy*, 224(Pt 3), 213–232. <https://doi.org/10.1111/j.1365-2818.2006.01706.x>
- Bray, F., Ferlay, J., Soerjomataram, I., Siegel, R. L., Torre, L. A., & Jemal, A. (2018). Global Cancer Statistics 2018: GLOBOCAN estimates of incidence and mortality worldwide for 36 cancers in 185 countries. *CA: A Cancer Journal for Clinicians*, 68(6), 394–424. <https://doi.org/10.3322/caac.21492>
- Bucci, C., Thomsen, P., Nicoziani, P., McCarthy, J., & van Deurs, B. (2000). Rab7: A key to lysosome biogenesis. *Molecular Biology of the Cell*, 11(2), 467–480. Retrieved from <https://doi.org/10.1091/mbc.11.2.467>
- Bustamante, H. A., Albornoz, N., Morselli, E., Soza, A., & Burgos, P. V. (2023). Novel insights into the non-canonical roles of PSMD14/POH1/Rpn11 in proteostasis and in the modulation of cancer progression. *Cellular Signalling*, 101, 110490. <https://doi.org/10.1016/j.cellsig.2022.110490>
- Bustamante, H. A., Cereceda, K., González, A. E., Valenzuela, G. E., Cheuquemilla, Y., Hernández, S., Arias-Muñoz, E., Cerda-Troncoso, C., Bandau, S., Soza, A., Kausel, G., Kerr, B., Mardones, G. A., Cancino, J., Hay, R. T., Rojas-Fernandez, A., & Burgos, P. V. (2020). The proteasomal deubiquitinating enzyme PSMD14 regulates macroautophagy by controlling Golgi-to-ER retrograde transport. *Cells*, 9(3), 777. <https://doi.org/10.3390/cells9030777>
- Cavieres, V. A., Cerda-Troncoso, C., Rivera-Dictter, A., Castro, R. I., Luchsinger, C., Santibañez, N., Burgos, P. V., & Mardones, G. A. (2020). Human Golgi phosphoprotein 3 is an effector of RAB1A and RAB1B. *PLoS one*, 15(8), e0237514. <https://doi.org/10.1371/journal.pone.0237514>
- Cerda-Troncoso, C. 2022. Decoding adaptive cellular mechanisms of cisplatin chemoresistance in ovarian cancer cells [Doctoral Thesis]. Universidad San Sebastián. Retrieved from <https://repositorio.uss.cl/handle/uss/8626>
- Chan, D. W., Lam, W. Y., Chen, F., Yung, M. M. H., Chan, Y. S., Chan, W. S., He, F., Liu, S. S., Chan, K. K. L., Li, B., & Ngan, H. Y. S. (2021). Genome-wide DNA methylome analysis identifies methylation signatures associated with survival and drug resistance of ovarian cancers. *Clinical Epigenetics*, 13(1), 142. <https://doi.org/10.1186/s13148-021-01130-5>
- Chen, S. H., & Chang, J. Y. (2019). New insights into mechanisms of cisplatin resistance: From tumor cell to microenvironment. *International Journal of Molecular Sciences*, 20(17), 4136. <https://doi.org/10.3390/ijms20174136>
- Chen, Y., Li, Y., Xiong, J., Lan, B., Wang, X., Liu, J., Lin, J., Fei, Z., Zheng, X., & Chen, C. (2021). Role of PRKDC in cancer initiation, progression, and treatment. *Cancer Cell International*, 21(1), 1–10. <https://doi.org/10.1186/s12935-021-02229-8>
- Dasari, S., & Tchounwou, P. B. (2014). Cisplatin in cancer therapy: Molecular mechanisms of action. *European Journal of Pharmacology*, 740, 364–378. <https://doi.org/10.1016/j.ejphar.2014.07.025>
- Dixon, A. C., Dawson, T. R., Di Vizio, D., & Weaver, A. M. (2023). Context-specific regulation of extracellular vesicle biogenesis and cargo selection. *Nature Reviews Molecular Cell Biology*, 24(7), 1–23. <https://doi.org/10.1038/s41580-023-00576-0>
- Dorayappan, K. D. P., Wanner, R., Wallbillich, J. J., Saini, U., Zingarelli, R., Suarez, A. A., Cohn, D. E., & Selvendiran, K. (2018). Hypoxia-induced exosomes contribute to a more aggressive and chemoresistant ovarian cancer phenotype: A novel mechanism linking STAT3/Rab proteins. *Oncogene*, 37(28), 3806–3821. <https://doi.org/10.1038/s41388-018-0189-0>
- Dozio, V., & Sanchez, J. C. (2017). Characterisation of extracellular vesicle-subsets derived from brain endothelial cells and analysis of their protein cargo modulation after TNF exposure. *Journal of Extracellular Vesicles*, 6(1), 1302705. <https://doi.org/10.1080/20013078.2017.1302705>
- Eitan, E., Suire, C., Zhang, S., & Mattson, M. P. (2016). Impact of lysosome status on extracellular vesicle content and release. *Ageing Research Reviews*, 32, 65–74. <https://doi.org/10.1016/j.arr.2016.05.001>
- Falguières, T., Luyet, P. P., Bissig, C., Scott, C. C., Velluz, M. C., & Gruenberg, J. (2008). In vitro budding of intraluminal vesicles into late endosomes is regulated by Alix and Tsg101. *Molecular Biology of the Cell*, 19(11), 4942–4955. <http://doi.org/10.1091/mbc.e08-03-0239>
- Fang, Z., Li, X., Wang, S., Jiang, Q., Loo, J. J., Jiang, X., Ju, L., Yu, H., Shen, T., Chen, M., Song, Y., Wang, Z., Du, X., & Liu, G. (2022). Overactivation of hepatic mechanistic target of rapamycin kinase complex 1 (mTORC1) is associated with low transcriptional activity of transcription factor EB and lysosomal dysfunction in dairy cows with clinical ketosis. *Journal of Dairy Science*, 105(5), 4520–4533. <https://doi.org/10.3168/jds.2021-20892>
- Ferreira, J. V., da Rosa Soares, A., Ramalho, J., Máximo Carvalho, C., Cardoso, M. H., Pintado, P., Carvalho, A. S., Beck, H. C., Matthesen, R., Zuzarte, M., Girão, H., van Niel, G., & Pereira, P. (2022). LAMP2A regulates the loading of proteins into exosomes. *Science Advances*, 8(12), eabm1140. <https://doi.org/10.1126/sciadv.abm1140>
- Galluzzi, L., Senovilla, L., Vitale, I., Michels, J., Martins, I., Kepp, O., Castedo, M., & Kroemer, G. (2012). Molecular mechanisms of cisplatin resistance. *Oncogene*, 31(15), 1869–1883. <https://doi.org/10.1038/onc.2011.384>
- Galluzzi, L., Vitale, I., Michels, J., Brenner, C., Szabadkai, G., Harel-Bellan, A., Castedo, M., & Kroemer, G. (2014). Systems biology of cisplatin resistance: Past, present and future. *Cell Death & Disease*, 5(5), e1257. <https://doi.org/10.1038/cddis.2013.428>
- Geisslinger, F., Müller, M., Vollmar, A. M., & Bartel, K. (2020). Targeting lysosomes in cancer as promising strategy to overcome chemoresistance—a mini review. *Frontiers in Oncology*, 10, 1–7. <https://doi.org/10.3389/fonc.2020.01156>
- Gerber, P. P., Cabrini, M., Jancic, C., Paoletti, L., Banchio, C., von Bilderling, C., Sigaut, L., Pietrasanta, L. I., Duette, G., Freed, E. O., Basile, G. d. S., Moita, C. F., Moita, L. F., Amigorena, S., Benaroch, P., Geffner, J., & Ostrowski, M. (2015). Rab27a controls HIV-1 assembly by regulating plasma membrane levels of phosphatidylinositol 4,5-bisphosphate. *The Journal of Cell Biology*, 209(3), 435–452. <https://doi.org/10.1083/jcb.201409082>
- Gremke, N., Polo, P., Dort, A., Schneikert, J., Elmshäuser, S., Brehm, C., Klingmüller, U., Schmitt, A., Reinhardt, H. C., Timofeev, O., Wanzel, M., & Stiewe, T. (2020). mTOR-mediated cancer drug resistance suppresses autophagy and generates a druggable metabolic vulnerability. *Nature Communications*, 11(1), 4684. <https://doi.org/10.1038/s41467-020-18504-7>
- Guerra, F., Paiano, A., Migoni, D., Girolimetti, G., Perrone, A. M., De Iaco, P., Fanizzi, F. P., Gasparre, G., & Bucci, C. (2019). Modulation of RAB7A protein expression determines resistance to cisplatin through late endocytic pathway impairment and extracellular vesicular secretion. *Cancers*, 11(1), 1–19. <https://doi.org/10.3390/cancers11010052>
- Guix, F. X., Capitán, A. M., Casadomé-Perales, Á., Palomares-Pérez, I., López Del Castillo, I., Miguel, V., Goedeke, L., Martín, M. G., Lamas, S., Peinado, H., Fernández-Hernando, C., & Dotti, C. G. (2021). Increased exosome secretion in neurons aging in vitro by NPC1-mediated endosomal cholesterol buildup. *Life Science Alliance*, 4(8), 1–18. <https://doi.org/10.26508/lsa.202101055>
- Helm, C. W., & States, J. C. (2009). Enhancing the efficacy of cisplatin in ovarian cancer treatment—Could arsenic have a role. *Journal of Ovarian Research*, 2, 1–7. <https://doi.org/10.1186/1757-2215-2-2>

- Hertzman Johansson, C., Azimi, A., Frostvik Stolt, M., Shojaee, S., Wiberg, H., Grafström, E., Hansson, J., & Egyházi Brage, S. (2013). Association of MITF and other melanosome-related proteins with chemoresistance in melanoma tumors and cell lines. *Melanoma Research*, 23(5), 360–365. <https://doi.org/10.1097/CMR.0b013e328362f9cd>
- Holzner, M., Hajdú, B., Lőrincz, T., Szarka, A., Bánhegyi, G., & Kapuy, O. (2020). Fine-tuning of AMPK-ULK1-mTORC1 regulatory triangle is crucial for autophagy oscillation. *Scientific Reports*, 10(1), 1–12. <https://doi.org/10.1038/s41598-020-75030-8>
- Homma, Y., Hiragi, S., & Fukuda, M. (2021). Rab family of small GTPases: An updated view on their regulation and functions. *The FEBS Journal*, 288(1), 36–55. <https://doi.org/10.1111/febs.15453>
- Huang, D., Li, G., Bhat, O. M., Zou, Y., Li, N., Ritter, J. K., & Li, P. L. (2022). Exosome biogenesis and lysosome function determine podocyte exosome release and glomerular inflammatory response during hyperhomocysteinemia. *The American Journal of Pathology*, 192(1), 43–55. <https://doi.org/10.1016/j.ajpath.2021.10.005>
- Huang, H., Hou, J., Liu, K., Liu, Q., Shen, L., Liu, B., Lu, Q., Zhang, N., Che, L., Li, J., Jiang, S., Wang, B., Wen, Q., Hu, L., & Gao, J. (2021). RAB27A-dependent release of exosomes by liver cancer stem cells induces Nanog expression in their differentiated progenies and confersregorafenib resistance. *Journal of Gastroenterology and Hepatology*, 36(12), 3429–3437. <https://doi.org/10.1111/jgh.15619>
- Huang, Z., Zhang, Y., Li, H., Zhou, Y., Zhang, Q., Chen, R., Jin, T., Hu, K., Li, S., Wang, Y., Chen, W., & Huang, Z. (2020). Correction: Vitamin D promotes the cisplatin sensitivity of oral squamous cell carcinoma by inhibiting LCN2-modulated NF- $\kappa$ B pathway activation through RPS3. *Cell Death & Disease*, 10(12), 1–14. <https://doi.org/10.1038/s41419-020-2389-0>
- Huotari, J., & Helenius, A. (2011). Endosome maturation. *The EMBO Journal*, 30(17), 3481–3500. <https://doi.org/10.1038/emboj.2011.286>
- Izco, M., Carlos, E., & Alvarez-Erviti, L. (2022). Impact of endolysosomal dysfunction upon exosomes in neurodegenerative diseases. *Neurobiology of Disease*, 166, 105651. <https://doi.org/10.1016/j.nbd.2022.105651>
- Jin, H., Tang, Y., Yang, L., Peng, X., Li, B., Fan, Q., Wei, S., Yang, S., Li, X., Wu, B., Huang, M., Tang, S., Liu, J., & Li, H. (2021). Rab GTPases: Central coordinators of membrane trafficking in cancer. *Frontiers in Cell and Developmental Biology*, 9, 1–13. <https://doi.org/10.3389/fcell.2021.648384>
- Kalayda, G. V., Wagner, C. H., Buss, I., Reedijk, J., & Jaehde, U. (2008). Altered localisation of the copper efflux transporters ATP7A and ATP7B associated with cisplatin resistance in human ovarian carcinoma cells. *BMC Cancer*, 8, 175. <https://doi.org/10.1186/1471-2407-8-175>
- Kametaka, S., Moriyama, K., Burgos, P. V., Eisenberg, E., Greene, L. E., Mattera, R., & Bonifacino, J. S. (2007). Canonical interaction of cyclin G associated kinase with adaptor protein 1 regulates lysosomal enzyme sorting. *Molecular Biology of the Cell*, 18(8), 2991–3001. <https://doi.org/10.1091/mbc.e06-12-1162>
- Kan, Y., Liu, J., & Li, F. (2020). High expression of nuclear transcription factor- $\kappa$ B is associated with cisplatin resistance and prognosis for ovarian cancer. *Cancer Management and Research*, 12, 8241–8252. <https://doi.org/10.2147/CMAR.S265531>
- Kelly, E. E., Horgan, C. P., Goud, B., & McCaffrey, M. W. (2012). The Rab family of proteins: 25 years on. *Biochemical Society Transactions*, 40(6), 1337–1347. <https://doi.org/10.1042/BST20120203>
- Kielbik, M., Krzyzanowski, D., Pawlik, B., & Klink, M. (2018). Cisplatin-induced ERK1/2 activity promotes G1 to S phase progression which leads to chemoresistance of ovarian cancer cells. *Oncotarget*, 9(28), 19847–19860. <https://doi.org/10.18632/oncotarget.24884>
- Kim, S., Han, Y., Kim, S. I., Kim, H. S., Kim, S. J., & Song, Y. S. (2018). Tumor evolution and chemoresistance in ovarian cancer. *NPJ Precision Oncology*, 2, 1–19. <https://doi.org/10.1038/s41698-018-0063-0>
- Klumperman, J., & Raposo, G. (2014). The complex ultrastructure of the endolysosomal system. *Cold Spring Harbor Perspectives in Biology*, 6(10), a016857–a016857. Retrieved from <https://doi.org/10.1101/cshperspect.a016857>
- Kobayashi, T., Sasaki, Y., Oshima, Y., Yamamoto, H., Mita, H., Suzuki, H., Toyota, M., Tokino, T., Itoh, F., Imai, K., & Shinomura, Y. (2006). Activation of the ribosomal protein L13 gene in human gastrointestinal cancer. *International Journal of Molecular Medicine*, 18(1), 161–170. <https://doi.org/10.3892/ijmm.18.1.161>
- Kobayashi, T., Vischer, U. M., Rosnoble, C., Lebrand, C., Lindsay, M., Parton, R. G., Kruithof, E. K., & Gruenberg, J. (2000). The tetraspanin CD63/lamp3 cycles between endocytic and secretory compartments in human endothelial cells. *Molecular Biology of the Cell*, 11(5), 1829–1843. <https://doi.org/10.1091/mbc.11.5.1829>
- Kubo, Y., Masumoto, H., Izumida, M., Kakoki, K., Hayashi, H., & Matsuyama, T. (2017). Rab3a-bound CD63 is degraded and Rab3a-Free CD63 is incorporated into HIV-1 particles. *Frontiers in Microbiology*, 8, 1–12. <https://doi.org/10.3389/fmicb.2017.01653>
- Kundu, S. T., Grzeskowiak, C. L., Fradette, J. J., Gibson, L. A., Rodriguez, L. B., Creighton, C. J., Scott, K. L., & Gibbons, D. L. (2018). TMEM106B drives lung cancer metastasis by inducing TFE3-dependent lysosome synthesis and secretion of cathepsins. *Nature Communications*, 9(1), 2731. <https://doi.org/10.1038/s41467-018-05013-x>
- Leblanc, R., Kashyap, R., Barral, K., Egea-Jimenez, A. L., Kovalsky, D., Feracci, M., Garcia, M., Derviaux, C., Betzi, S., Ghossoub, R., Platonov, M., Roche, P., Morelli, X., Hoffer, L., & Zimmermann, P. (2020). Pharmacological inhibition of syntenin PDZ2 domain impairs breast cancer cell activities and exosome loading with syndecan and EpCAM cargo. *Journal of Extracellular Vesicles*, 10(2), e12039. <https://doi.org/10.1002/jev2.12039>
- Lee, J. T., & Gu, W. (2010). The multiple levels of regulation by p53 ubiquitination. *Cell Death and Differentiation*, 17(1), 86–92. <https://doi.org/10.1038/cdd.2009.77>
- Lehrich, B. M., Liang, Y., & Fiandaca, M. S. (2021). Foetal bovine serum influence on in vitro extracellular vesicle analyses. *Journal of Extracellular Vesicles*, 10(3), e12061. <https://doi.org/10.1002/jev2.12061>
- Li, J., Jin, Q., Huang, F., Tang, Z., & Huang, J. (2017). Effects of Rab27A and Rab27B on invasion, proliferation, apoptosis, and chemoresistance in human pancreatic cancer cells. *Pancreas*, 46(9), 1173–1179. <https://doi.org/10.1097/MPA.0000000000000910>
- Li, M., Chen, D., Shiloh, A., Luo, J., Nikolaev, A. Y., Qin, J., & Gu, W. (2002). Deubiquitination of p53 by HAUSP is an important pathway for p53 stabilization. *Nature*, 416(6881), 648–653. <https://doi.org/10.1038/nature737>
- Li, X., Wang, H., Ni, Q., Tang, Z., Ni, J., Xu, L., Huang, H., Ni, S., & Feng, J. (2017). Effects of silencing Rab27a gene on biological characteristics and chemosensitivity of non-small cell lung cancer. *Oncotarget*, 8(55), 94481–94492. <https://doi.org/10.18632/oncotarget.21782>
- Liu, C., He, X., Liu, X., Yu, J., Zhang, M., Yu, F., & Wang, Y. (2019). RPS15A promotes gastric cancer progression via activation of the Akt/IKK- $\beta$ /NF- $\kappa$ B signalling pathway. *Journal of Cellular and Molecular Medicine*, 23(3), 2207–2218. <https://doi.org/10.1111/jcmm.14141>
- Liu, J., Gong, X., Zhu, X., Xue, D., Liu, Y., & Wang, P. (2017). Rab27A overexpression promotes bladder cancer proliferation and chemoresistance through regulation of NF- $\kappa$ B signaling. *Oncotarget*, 8(43), 75272–75283. <https://doi.org/10.18632/oncotarget.20775>
- Liu, J., Zhang, L., Zhang, X., & Xing, X. (2015). Rapamycin enhanced the antitumor efficacy of oxaliplatin in cisplatin-resistant ovarian cancer cells A2780cis both in vitro and in vivo. *Journal of Chemotherapy (Florence, Italy)*, 27(6), 358–364. <https://doi.org/10.1179/1973947815Y.0000000021>
- Ma, Q., Yang, F., Mackintosh, C., Jayani, R. S., Oh, S., Jin, C., Nair, S. J., Merkurjev, D., Ma, W., Allen, S., Wang, D., Almenar-Queralt, A., & Garcia-Bassets, I. (2020). Super-enhancer redistribution as a mechanism of broad gene dysregulation in repeatedly drug-treated cancer cells. *Cell Reports*, 31(3), 107532. <https://doi.org/10.1016/j.celrep.2020.107532>
- Mad-Adam, N., Rattanaburee, T., Tanawattanasuntorn, T., & Graidist, P. (2022). Effects of trans-( $\pm$ )-kusunokinin on chemosensitive and chemoresistant ovarian cancer cells. *Oncology Letters*, 23(2), 59. <https://doi.org/10.3892/ol.2021.13177>



- Madden, E. C., Gorman, A. M., Logue, S. E., & Samali, A. (2020). Tumour cell secretome in chemoresistance and tumour recurrence. *Trends in Cancer*, 6(6), 489–505. <https://doi.org/10.1016/j.trecan.2020.02.020>
- Mardones, G. A., Burgos, P. V., Brooks, D. A., Parkinson-Lawrence, E., Mattera, R., & Bonifacino, J. S. (2007). The trans-Golgi network accessory protein p56 promotes long-range movement of GGA/clathrin-containing transport carriers and lysosomal enzyme sorting. *Molecular Biology of the Cell*, 18(9), 3486–3501. <https://doi.org/10.1091/mbc.e07-02-0190>
- Mathieu, M., Névo, N., Jouve, M., Valenzuela, J. I., Maurin, M., Verweij, F. J., Palmulli, R., Lankar, D., Dingli, F., Loew, D., Rubinstein, E., Boncompain, G., Perez, F., & Théry, C. (2021). Specificities of exosome versus small ectosome secretion revealed by live intracellular tracking of CD63 and CD9. *Nature Communications*, 12(1), 4389. <https://doi.org/10.1038/s41467-021-24384-2>
- Merten, O. W., Hebben, M., & Bovolenta, C. (2016). Production of lentiviral vectors. *Molecular Therapy Methods & Clinical Development*, 3, 16017. <https://doi.org/10.1038/mtm.2016.17>
- Messenger, S. W., Woo, S. S., Sun, Z., & Martin, T. F. J. (2018). A Ca<sup>2+</sup>-stimulated exosome release pathway in cancer cells is regulated by Munc13-4. *The Journal of Cell Biology*, 217(8), 2877–2890. <https://doi.org/10.1083/jcb.201710132>
- Miranda, A. M., Lasiecka, Z. M., Xu, Y., Neufeld, J., Shahriar, S., Simoes, S., Chan, R. B., Oliveira, T. G., Small, S. A., & Di Paolo, G. (2018). Neuronal lysosomal dysfunction releases exosomes harboring APP C-terminal fragments and unique lipid signatures. *Nature Communications*, 9(1), 291. <https://doi.org/10.1038/s41467-017-02533-w>
- Moon, S., Shin, D. W., Kim, S., Lee, Y. S., Mankhong, S., Yang, S. W., Lee, P. H., Park, D. H., Kwak, H. B., Lee, J. S., & Kang, J. H. (2019). Enrichment of exosome-like extracellular vesicles from plasma suitable for clinical vesicular miRNA biomarker research. *Journal of Clinical Medicine*, 8(11), 1995. <https://doi.org/10.3390/jcm8111995>
- Nguyen, E. V., Huhtinen, K., Goo, Y. A., Kaipio, K., Andersson, N., Rantanen, V., Hynninen, J., Lahesmaa, R., Carpen, O., & Goodlett, D. R. (2017). Hyperphosphorylation of sequestosome-1 distinguishes resistance to cisplatin in patient derived high grade serous ovarian cancer cells. *Molecular & Cellular Proteomics: MCP*, 16(7), 1377–1392. <https://doi.org/10.1074/mcp.M116.058321>
- Norouzi-Barough, L., Sarookhani, M. R., Sharifi, M., Moghbelinejad, S., Jangjoo, S., & Salehi, R. (2018). Molecular mechanisms of drug resistance in ovarian cancer. *Journal of Cellular Physiology*, 233(6), 4546–4562. <https://doi.org/10.1002/jcp.26289>
- Oberle, C., Huai, J., Reinheckel, T., Tacke, M., Rassner, M., Ekert, P. G., Buelllesbach, J., & Borner, C. (2010). Lysosomal membrane permeabilization and cathepsin release is a Bax/Bak-dependent, amplifying event of apoptosis in fibroblasts and monocytes. *Cell Death and Differentiation*, 17(7), 1167–1178. <https://doi.org/10.1038/cdd.2009.214>
- O’Dea, R. F., Mirkin, B. L., Alward, C. T., & Sinaiko, A. R. (1988). Treatment of neonatal hypertension with captopril. *The Journal of Pediatrics*, 113(2), 403–406. [https://doi.org/10.1016/s0022-3476\(88\)80292-0](https://doi.org/10.1016/s0022-3476(88)80292-0)
- Ostrowski, M., Carmo, N. B., Krumeich, S., Fanget, I., Raposo, G., Savina, A., Moita, C. F., Schauer, K., Hume, A. N., Freitas, R. P., Goud, B., Benaroch, P., Hacohen, N., Fukuda, M., Desnos, C., Seabra, M. C., Darchen, F., Amigorena, S., Moita, L. F., & Thery, C. (2010). Rab27a and Rab27b control different steps of the exosome secretion pathway. *Nature Cell Biology*, 12(1), 19–30. <https://doi.org/10.1038/ncb2000>
- Palmieri, M., Impey, S., Kang, H., di Ronza, A., Pelz, C., Sardiello, M., & Ballabio, A. (2011). Characterization of the CLEAR network reveals an integrated control of cellular clearance pathways. *Human Molecular Genetics*, 20(19), 3852–3866. <https://doi.org/10.1093/hmg/ddr306>
- Patch, A. M., Christie, E. L., Etemadmoghadam, D., Garsed, D. W., George, J., Fereday, S., Nones, K., Cowin, P., Alsop, K., Bailey, P. J., Kassahn, K. S., Newell, F., Quinn, M. C., Kazakoff, S., Quek, K., Wilhelm-Benartzi, C., Curry, E., Leong, H. S., Australian Ovarian Cancer Study Group. ... Bowtell, D. D. (2015). Whole-genome characterization of chemoresistant ovarian cancer. *Nature*, 521(7553), 489–494. <https://doi.org/10.1038/nature14410>
- Peng, X., Yang, L., Ma, Y., Li, X., Yang, S., Li, Y., Wu, B., Tang, S., Zhang, F., Zhang, B., Liu, J., & Li, H. (2021). IKK $\beta$  activation promotes amphisome formation and extracellular vesicle secretion in tumor cells. *Biochimica Et Biophysica Acta Molecular Cell Research*, 1868(1), 118857. <https://doi.org/10.1016/j.bbamcr.2020.118857>
- Pi, H., Li, M., Tian, L., Yang, Z., Yu, Z., & Zhou, Z. (2016). Enhancing lysosomal biogenesis and autophagic flux by activating the transcription factor EB protects against cadmium-induced neurotoxicity. *Scientific Reports*, 7, 1–14. <https://doi.org/10.1038/srep43466>
- Piletic, K., Alsaleh, G., & Simon, A. K. (2023). Autophagy orchestrates the crosstalk between cells and organs. *EMBO Reports*, 24(9), e57289.
- Qin, S., Jiang, J., Lu, Y., Nice, E. C., Huang, C., Zhang, J., & He, W. (2020). Emerging role of tumor cell plasticity in modifying therapeutic response. *Signal Transduction and Targeted Therapy*, 5(1), 228. <https://doi.org/10.1038/s41392-020-00313-5>
- Quinney, K. B., Frankel, E. B., Shankar, R., Kasberg, W., Luong, P., & Audhya, A. (2019). Growth factor stimulation promotes multivesicular endosome biogenesis by prolonging recruitment of the late-acting ESCRT machinery. *Proceedings of the National Academy of Sciences of the United States of America*, 116(14), 6858–6867. <https://doi.org/10.1073/pnas.1817898116>
- Reid, B. M., Permuth, J. B., & Sellers, T. A. (2017). Epidemiology of ovarian cancer: A review. *Cancer Biology & Medicine*, 14(1), 9–32. <https://doi.org/10.20892/j.issn.2095-3941.2016.0084>
- Rosner, M., Schipany, K., & Hengstschlager, M. (2012). p70 S6K1 nuclear localization depends on its mTOR-mediated phosphorylation at T389, but not on its kinase activity towards S6. *Amino Acids*, 42(6), 2251–2256. <https://doi.org/10.1007/s00726-011-0965-4>
- Rouillard, A. D., Gundersen, G. W., Fernandez, N. F., Wang, Z., Monteiro, C. D., McDermott, M. G., & Ma’ayan, A. (2016). The harmonizome: a collection of processed datasets gathered to serve and mine knowledge about genes and proteins. *Database: The Journal of Biological Databases and Curation*, 2016, baw100. <https://doi.org/10.1093/database/baw100>
- Safaei, R., Larson, B. J., Cheng, T. C., Gibson, M. A., Otani, S., Naerdemann, W., & Howell, S. B. (2005). Abnormal lysosomal trafficking and enhanced exosomal export of cisplatin in drug-resistant human ovarian carcinoma cells. *Molecular Cancer Therapeutics*, 4(10), 1595–1604. <https://doi.org/10.1158/1535-7163.MCT-05-0102>
- Saftig, P., & Klumperman, J. (2009). Lysosome biogenesis and lysosomal membrane proteins: trafficking meets function. *Nature Reviews Molecular Cell Biology*, 10(9), 623–635. <https://doi.org/10.1038/nrm2745>
- Salimu, J., Webber, J., Gurney, M., Al-Taei, S., Clayton, A., & Tabi, Z. (2017). Dominant immunosuppression of dendritic cell function by prostate-cancer-derived exosomes. *Journal of Extracellular Vesicles*, 6(1), 1368823. <https://doi.org/10.1080/20013078.2017.1368823>
- Schindelin, J., Arganda-Carreras, I., Frise, E., Kaynig, V., Longair, M., Pietzsch, T., Preibisch, S., Rueden, C., Saalfeld, S., Schmid, B., Tinevez, J. Y., White, D. J., Hartenstein, V., Eliceiri, K., Tomancak, P., & Cardona, A. (2012). Fiji: an open-source platform for biological-image analysis. *Nature Methods*, 9(7), 676–682. <https://doi.org/10.1038/nmeth.2019>
- Sears, C. R., & Turchi, J. J. (2012). Complex cisplatin-double strand break (DSB) lesions directly impair cellular non-homologous end-joining (NHEJ) independent of downstream damage response (DDR) pathways. *The Journal of Biological Chemistry*, 287(29), 24263–24272. <https://doi.org/10.1074/jbc.M112.344911>



- Settembre, C., Zoncu, R., Medina, D. L., Vetrini, F., Erdin, S., Huynh, T., Ferron, M., Karsenty, G., Vellard, M. C., Facchinetti, V., Sabatini, D. M., & Ballabio, A. (2012). A lysosome-to-nucleus signalling mechanism senses and regulates the lysosome via mTOR and TFEB. *The EMBO Journal*, 31(5), 1095–1108. <https://doi.org/10.1038/emboj.2012.32>
- Shen, D. W., Pouliot, L. M., Hall, M. D., & Gottesman, M. M. (2012). Cisplatin resistance: A cellular self-defense mechanism resulting from multiple epigenetic and genetic changes. *Pharmacological Reviews*, 64(3), 706–721. <https://doi.org/10.1124/pr.111.005637>
- Shi, Z., Wu, D., Xu, H., Yang, J., & Sun, X. (2021). CSNK2A1-mediated phosphorylation of HMGGA2 modulates cisplatin resistance in cervical cancer. *FEBS Open Bio*, 11(8), 2245–2255. <https://doi.org/10.1002/2211-5463.13228>
- Shin, H. R., & Zoncu, R. (2020). The lysosome at the intersection of cellular growth and destruction. *Developmental Cell*, 54(2), 226–238. <https://doi.org/10.1016/j.devcel.2020.06.010>
- Shinde, S. R., & Maddika, S. (2018). Post translational modifications of Rab GTPases. *Small GTPases*, 9(1-2), 49–56. <https://doi.org/10.1080/21541248.2017.1299270>
- Song, L., Tang, S., Han, X., Jiang, Z., Dong, L., Liu, C., Liang, X., Dong, J., Qiu, C., Wang, Y., & Du, Y. (2019). KIBRA controls exosome secretion via inhibiting the proteasomal degradation of Rab27a. *Nature Communications*, 10(1), 1639. <https://doi.org/10.1038/s41467-019-09720-x>
- Steinbichler, T. B., Dudás, J., Skvortsov, S., Ganswindt, U., Riechelmann, H., & Skvortsova, I. I. (2019). Therapy resistance mediated by exosomes. *Molecular Cancer*, 18(1), 1–11. <https://doi.org/10.1186/s12943-019-0970-x>
- Sun, M. Y., Xu, B., Wu, Q. X., Chen, W. L., Cai, S., Zhang, H., & Tang, Q. F. (2021). Cisplatin-resistant gastric cancer cells promote the chemoresistance of cisplatin-sensitive cells via the exosomal RPS3-mediated PI3K-Akt-Cofilin-1 signaling axis. *Frontiers in Cell and Developmental Biology*, 9, 618899. <https://doi.org/10.3389/fcell.2021.618899>
- Sung, H., Ferlay, J., Siegel, R. L., Laversanne, M., Soerjomataram, I., Jemal, A., & Bray, F. (2021). Global Cancer Statistics 2020: GLOBOCAN estimates of incidence and mortality worldwide for 36 cancers in 185 countries. *CA: A Cancer Journal for Clinicians*, 71(3), 209–249. <https://doi.org/10.3322/caac.21660>
- Tchounwou, P. B., Dasari, S., Noubissi, F. K., Ray, P., & Kumar, S. (2021). Advances in our understanding of the molecular mechanisms of action of cisplatin in cancer therapy. *Journal of Experimental Pharmacology*, 13, 303–328. <https://doi.org/10.2147/JEP.S267383>
- Théry, C., Witwer, K. W., Aikawa, E., Alcaraz, M. J., Anderson, J. D., Andriantsitohaina, R., Antoniou, A., Arab, T., Archer, F., Atkin-Smith, G. K., Ayre, D. C., Bach, J. M., Bachurski, D., Baharvand, H., Balaj, L., Baldacchino, S., Bauer, N. N., Baxter, A. A., Bebawy, M., ... Zuba-Surma, E. K. (2018). Minimal information for studies of extracellular vesicles 2018 (MISEV2018): A position statement of the International Society for Extracellular Vesicles and update of the MISEV2014 guidelines. *Journal of Extracellular Vesicles*, 7(1), 1535750. <https://doi.org/10.1080/20013078.2018.1535750>
- Tian, W., Lei, N., Zhou, J., Chen, M., Guo, R., Qin, B., Li, Y., & Chang, L. (2022). Extracellular vesicles in ovarian cancer chemoresistance, metastasis, and immune evasion. *Cell Death & Disease*, 13(1), 64. <https://doi.org/10.1038/s41419-022-04510-8>
- Tong, X., Zhao, J., Zhang, Y., Mu, P., & Wang, X. (2019). Expression levels of MRP1, GST- $\pi$ , and GSK3 $\beta$  in ovarian cancer and the relationship with drug resistance and prognosis of patients. *Oncology Letters*, 18(1), 22–28. <https://doi.org/10.3892/ol.2019.10315>
- Traer, C. J., Rutherford, A. C., Palmer, K. J., Wassmer, T., Oakley, J., Attar, N., Carlton, J. G., Kremerskothen, J., Stephens, D. J., & Cullen, P. J. (2007). SNX4 coordinates endosomal sorting of TfnR with dynein-mediated transport into the endocytic recycling compartment. *Nature Cell Biology*, 9(12), 1370–1380. <https://doi.org/10.1186/10.1038/ncb1656>
- Trivedi, P. C., Bartlett, J. J., & Pulinilkunnil, T. (2020). Lysosomal biology and function: Modern view of cellular debris bin. *Cells*, 9(5), 1–35. <https://doi.org/10.3390/cells9051131>
- van de Vlekkert, D., Demmers, J., Nguyen, X. X., Campos, Y., Machado, E., Annunziata, I., Hu, H., Gomero, E., Qiu, X., Bongiovanni, A., Feghali-Bostwick, C. A., & d'Azzo, A. (2019). Excessive exosome release is the pathogenic pathway linking a lysosomal deficiency to generalized fibrosis. *Science Advances*, 5(7), eaav3270. <https://doi.org/10.1126/sciadv.aav3270>
- van Jaarsveld, M. T. M., Deng, D., Ordoñez-Rueda, D., Paulsen, M., Wiemer, E. A. C., & Zi, Z. (2020). Cell-type-specific role of CHK2 in mediating DNA damage-induced G2 cell cycle arrest. *Oncogenesis*, 9(3), 1–7. <https://doi.org/10.1186/10.1038/s41389-020-0219-y>
- Vanlandingham, P. A., & Ceresa, B. P. (2009). Rab7 regulates late endocytic trafficking downstream of multivesicular body biogenesis and cargo sequestration. *The Journal of Biological Chemistry*, 284(18), 12110–12124. <https://doi.org/10.1074/jbc.M809277200>
- Vanlandingham, P. A., & Ceresa, B. P. (2009). Rab7 regulates late endocytic trafficking downstream of multivesicular body biogenesis and cargo sequestration. *The Journal of Biological Chemistry*, 284(18), 12110–12124. <https://doi.org/10.1074/jbc.M809277200>
- van Niel, G., D'Angelo, G., & Raposo, G. (2018). Shedding light on the cell biology of extracellular vesicles. *Nature Reviews Molecular Cell Biology*, 19(4), 213–228. <https://doi.org/10.1038/nrm.2017.125>
- Varas-Godoy, M., Lladser, A., Farfan, N., Villota, C., Villegas, J., Tapia, J. C., Burzio, L. O., Burzio, V. A., & Valenzuela, P. D. T. (2018). In vivo knockdown of antisense non-coding mitochondrial RNAs by a lentiviral-encoded shRNA inhibits melanoma tumor growth and lung colonization. *Pigment Cell & Melanoma Research*, 31(1), 64–72. <https://doi.org/10.1111/pcmr.12615>
- Vargas, G., Cortés, O., Arias-Muñoz, E., Hernández, S., Cerda-Troncoso, C., Hernández, L., González, A. E., Tatham, M. H., Bustamante, H. A., Retamal, C., Cancino, J., Varas-Godoy, M., Hay, R. T., Rojas-Fernández, A., Cavieres, V. A., & Burgos, P. V. (2022). Negative modulation of macroautophagy by stabilized HERPUD1 is counteracted by an increased ER-lysosomal network with impact in drug-induced stress cell survival. *Frontiers in Cell and Developmental Biology*, 10, 1–22. <https://doi.org/10.3389/fcell.2022.743287>
- Vera, N., Acuña-Gallardo, S., Grünwald, F., Caceres-Verschae, A., Realini, O., Acuña, R., Lladser, A., Illanes, S. E., & Varas-Godoy, M. (2019). Small extracellular vesicles released from ovarian cancer spheroids in response to cisplatin promote the pro-tumorigenic activity of mesenchymal stem cells. *International Journal of Molecular Sciences*, 20(20), 4972. <https://doi.org/10.3390/ijms20204972>
- Verderio, C., Gabrielli, M., & Giussani, P. (2018). Role of sphingolipids in the biogenesis and biological activity of extracellular vesicles. *Journal of Lipid Research*, 59(8), 1325–1340. <https://doi.org/10.1194/jlr.R083915>
- Verweij, F. J., Bebelman, M. P., George, A. E., Couty, M., Bécot, A., Palmulli, R., Heiligenstein, X., Sirés-Campos, J., Raposo, G., Pegtel, D. M., & van Niel, G. (2022). ER membrane contact sites support endosomal small GTPase conversion for exosome secretion. *The Journal of Cell Biology*, 221(12), e202112032. <https://doi.org/10.1083/jcb.202112032>
- Villarroya-Beltri, C., Baixauli, F., Mittelbrunn, M., Fernández-Delgado, I., Torralba, D., Moreno-Gonzalo, O., Baldanta, S., Enrich, C., Guerra, S., & Sánchez-Madrid, F. (2016). ISGylation controls exosome secretion by promoting lysosomal degradation of MVB proteins. *Nature Communications*, 7, 13588. <https://doi.org/10.1038/ncomms13588>
- Wang, J., Liu, Q., Zhao, Y., Fu, J., & Su, J. (2023). Tumor cells transmit drug resistance via cisplatin-induced extracellular vesicles. *International Journal of Molecular Sciences*, 24(15), 12347. <https://doi.org/10.3390/ijms241512347>
- Wang, L., Valiskova, B., & Forejt, J. (2018). Cisplatin-induced DNA double-strand breaks promote meiotic chromosome synapsis in PRDM9-controlled mouse hybrid sterility. *Elife*, 7, e42511. <https://doi.org/10.7554/eLife.42511>

- Wang, T., Gilkes, D. M., Takano, N., Xiang, L., Luo, W., Bishop, C. J., Chaturvedi, P., Green, J. J., & Semenza, G. L. (2014). Hypoxia-inducible factors and RAB22A mediate formation of microvesicles that stimulate breast cancer invasion and metastasis. *Proceedings of the National Academy of Sciences of the United States of America*, *111*(31), E3234–E3242. <https://doi.org/10.1073/pnas.1410041111>
- Wang, X., Qiao, D., Chen, L., Xu, M., Chen, S., Huang, L., Wang, F., Chen, Z., Cai, J., & Fu, L. (2019). Chemotherapeutic drugs stimulate the release and recycling of extracellular vesicles to assist cancer cells in developing an urgent chemoresistance. *Molecular Cancer*, *18*(1), 1–18. <https://doi.org/10.1186/s12943-019-1114-z>
- Wei, D., Zhan, W., Gao, Y., Huang, L., Gong, R., Wang, W., Zhang, R., Wu, Y., Gao, S., & Kang, T. (2021). RAB31 marks and controls an ESCRT-independent exosome pathway. *Cell Research*, *31*(2), 157–177. <https://doi.org/10.1038/s41422-020-00409-1>
- White, I. J., Bailey, L. M., Aghakhani, M. R., Moss, S. E., & Futter, C. E. (2006). EGF stimulates annexin 1-dependent inward vesiculation in a multivesicular endosome subpopulation. *The EMBO Journal*, *25*(1), 1–12. <https://doi.org/10.1038/sj.emboj.7600759>
- Williams, A. B., & Schumacher, B. (2016). p53 in the DNA-damage-repair process. *Cold Spring Harbor Perspectives in Medicine*, *6*(5), a026070. <https://doi.org/10.1101/cshperspect.a026070>
- Wiśniewski, J. R., Zougman, A., Nagaraj, N., & Mann, M. (2009). Universal sample preparation method for proteome analysis. *Nature Methods*, *6*(5), 359–362. <https://doi.org/10.1038/nmeth.1322>
- Wollert, T., & Hurley, J. H. (2010). Molecular mechanism of multivesicular body biogenesis by ESCRT complexes. *Nature*, *464*(7290), 864–869. <https://doi.org/10.1038/nature08849>
- Xavier, C. P. R., Belisario, D. C., Rebelo, R., Assaraf, Y. G., Giovannetti, E., Kopecka, J., & Vasconcelos, M. H. (2022). The role of extracellular vesicles in the transfer of drug resistance competences to cancer cells. *Drug Resistance Updates: Reviews and Commentaries in Antimicrobial and Anticancer Chemotherapy*, *62*, 100833. <https://doi.org/10.1016/j.drug.2022.100833>
- Xie, W., Sun, H., Li, X., Lin, F., Wang, Z., & Wang, X. (2021). Ovarian cancer: Epigenetics, drug resistance, and progression. *Cancer Cell International*, *21*(1), 1–16. <https://doi.org/10.1186/s12935-021-02136-y>
- Xu, D., Tang, W. J., Zhu, Y. Z., Liu, Z., Yang, K., Liang, M. X., Chen, X., Wu, Y., Tang, J. H., & Zhang, W. (2022). Hyperthermia promotes exosome secretion by regulating Rab7b while increasing drug sensitivity in adriamycin-resistant breast cancer. *International Journal of Hyperthermia: the Official Journal of European Society for Hyperthermic Oncology, North American Hyperthermia Group*, *39*(1), 246–257. <https://doi.org/10.1080/02656736.2022.2029585>
- Xu, J., Yang, K. C., Go, N. E., Colborne, S., Ho, C. J., Hosseini-Beheshti, E., Lystad, A. H., Simonsen, A., Guns, E. T., Morin, G. B., & Gorski, S. M. (2022). Chloroquine treatment induces secretion of autophagy-related proteins and inclusion of Atg8-family proteins in distinct extracellular vesicle populations. *Autophagy*, *18*(11), 2547–2560. <https://doi.org/10.1080/15548627.2022.2039535>
- Yáñez-Mó, M., Siljander, P. R., Andreu, Z., Zavec, A. B., Borràs, F. E., Buzas, E. I., Buzas, K., Casal, E., Cappello, F., Carvalho, J., Colás, E., Cordeiro-da Silva, A., Fais, S., Falcon-Perez, J. M., Ghobrial, I. M., Giebel, B., Gimona, M., Graner, M., Gursel, I., ... De Wever, O. (2015). Biological properties of extracellular vesicles and their physiological functions. *Journal of Extracellular Vesicles*, *4*, 27066. <https://doi.org/10.3402/jev.v4.27066>
- Yang, C., & Wang, X. (2021). Lysosome biogenesis: Regulation and functions. *The Journal of Cell Biology*, *220*(6), 1–15. <https://doi.org/10.1083/jcb.202102001>
- Yang, E., Wang, X., Gong, Z., Yu, M., Wu, H., & Zhang, D. (2020). Exosome-mediated metabolic reprogramming: The emerging role in tumor microenvironment remodeling and its influence on cancer progression. *Signal Transduction and Targeted Therapy*, *5*(1), 1–13. <https://doi.org/10.1038/s41392-020-00359-5>
- Yu, W., Li, L., Wang, G., Zhang, W., Xu, J., & Liang, A. (2018). KU70 inhibition impairs both non-homologous end joining and homologous recombination DNA damage repair through SHP-1 induced dephosphorylation of SIRT1 in T-cell acute lymphoblastic leukemia (T-ALL) [corrected]. *Cellular Physiology and Biochemistry: International Journal of Experimental Cellular Physiology, Biochemistry, and Pharmacology*, *49*(6), 2111–2123. <https://doi.org/10.1159/000493815>
- Zerial, M., & McBride, H. (2001). Rab proteins as membrane organizers. *Nature Reviews Molecular Cell Biology*, *2*(2), 107–117. <https://doi.org/10.1038/35052055>
- Zhai, X., & El Hiani, Y. (2020). Getting lost in the cell-lysosomal entrapment of chemotherapeutics. *Cancers*, *12*(12), 1–21. <https://doi.org/10.3390/cancers12123669>
- Zhang, H., Lu, J., Liu, J., Zhang, G., & Lu, A. (2020). Advances in the discovery of exosome inhibitors in cancer. *Journal of Enzyme Inhibition and Medicinal Chemistry*, *35*(1), 1322–1330. <https://doi.org/10.1080/14756366.2020.1754814>
- Zhang, J., Tan, J., Wang, M., Wang, Y., Dong, M., Ma, X., Sun, B., Liu, S., Zhao, Z., Chen, L., Liu, K., Xin, Y., & Zhuang, L. (2021). Lipid-induced DRAM recruits STOM to lysosomes and induces LMP to promote exosome release from hepatocytes in NAFLD. *Science Advances*, *7*(45), eabh1541. <https://doi.org/10.1126/sciadv.abh1541>
- Zhang, J., Willers, H., Feng, Z., Ghosh, J. C., Kim, S., Weaver, D. T., Chung, J. H., Powell, S. N., & Xia, F. (2004). Chk2 phosphorylation of BRCA1 regulates DNA double-strand break repair. *Molecular and Cellular Biology*, *24*(2), 708–718. <https://doi.org/10.1128/MCB.24.2.708-718.2004>
- Zhao, W., Li, X., Nian, W., Wang, J., Wang, X., Sun, L., Zhu, Y., & Tong, Z. (2021). Ribosome proteins represented by RPL27A mark the development and metastasis of triple-negative breast cancer in mouse and human. *Frontiers in Cell and Developmental Biology*, *9*, 716730. <https://doi.org/10.3389/fcell.2021.716730>
- Zhitomirsky, B., & Assaraf, Y. G. (2016). Lysosomes as mediators of drug resistance in cancer. *Drug Resistance Updates: Reviews and Commentaries in Antimicrobial and Anticancer Chemotherapy*, *24*, 23–33. <https://doi.org/10.1016/j.drug.2015.11.004>
- Zuo, R., Liu, M., Wang, Y., Li, J., Wang, W., Wu, J., Sun, C., Li, B., Wang, Z., Lan, W., Zhang, C., Shi, C., & Zhou, Y. (2020). Correction to: BM-MSC-derived exosomes alleviate radiation-induced bone loss by restoring the function of recipient BM-MSCs and activating Wnt/ $\beta$ -catenin signaling. *Stem Cell Research & Therapy*, *11*(1), 33. <https://doi.org/10.1186/s13287-020-1553-x>

## SUPPORTING INFORMATION

Additional supporting information can be found online in the Supporting Information section at the end of this article.

**How to cite this article:** Cerda-Troncoso, C., Grünenwald, F., Arias-Muñoz, E., Cavieres, V. A., Caceres-Verschae, A., Hernández, S., Gaete-Ramírez, B., Álvarez-Astudillo, F., Acuña, R. A., Ostrowski, M., Burgos, P. V., & Varas-Godoy, M. (2024). Chemo-small extracellular vesicles released in cisplatin-resistance ovarian cancer cells are regulated by the lysosomal function. *Journal of Extracellular Biology*, *3*, e157. <https://doi.org/10.1002/jex2.157>